Investigation of inactive state κ opioid receptor homodimerization via single molecule microscopy using new antagonistic fluorescent probes

Drakopoulos, Antonios; Koszegi, Zsombor; Lanoiselee, Yann; Hubner, Harald; Gmeiner, Peter; Calebiro, Davide; Decker, Michael

Document Version
Peer reviewed version

Link to publication on Research at Birmingham portal

Investigation of inactive state κ opioid receptor homodimerization via single molecule microscopy using new antagonistic fluorescent probes

Antonios Drakopoulos[+], Zsombor Koszegi[#], Yann Lanoiselée[#], Harald Hübner[§], Peter Gmeiner[§], Davide Calebiro*[#], Michael Decker*[+].

+: Pharmaceutical and Medicinal Chemistry, Institute of Pharmacy and Food Chemistry, Julius Maximilian University of Würzburg, 97074 Würzburg, Germany

#: Institute of Metabolism and Systems Research and Centre of Membrane Proteins and Receptors, College of Medical and Dental Sciences, University of Birmingham, B152TT Birmingham, United Kingdom

§: Medicinal Chemistry, Department of Chemistry and Pharmacy, Friedrich-Alexander University of Erlangen-Nürnberg, 91058 Erlangen, Germany

KEYWORDS: fluorescent probe, 5'-guanidinonaltrindole, TIRF, Single Molecule Microscopy, GPCR.

ABSTRACT: Opioid receptors (ORs) are among the best studied G protein-coupled receptors (GPCRs) due to their involvement in neurological disorders and important role in pain treatment. Contrary to the classical monomeric model, indirect evidence suggests that ORs might form dimers, which could be endowed with a distinct pharmacological profile, and, thus, be targeted to develop innovative pharmacological therapies. However, direct evidence for the spontaneous formation of OR dimers in living cells under physiological conditions is missing. Despite a growing interest in the kappa opiod receptor (KOR), KOR-selective fluorescent probes are particularly scarce in literature. Herein, we present the first set of fluorescent KOR-selective probes with antagonistic properties. Two of these were employed in single molecule microscopy (SMM) experiments to investigate KOR homodimerization, localization and trafficking. Our findings indicate that most KORs labelled with the new fluorescent probes are present as apparently freely diffusing monomers on the surface of a simple cell model.

Introduction

Opioid drugs remain, in spite of severe side effects such as respiratory depression and addiction, among the most commonly prescribed pain relievers and broad-spectrum analgesics due to their clinical efficacy.[1–6] Opioids produce their pharmacological actions by binding to specific receptors located at the surface of neurons. Opioid receptors (ORs)[7] are divided in three classical subtypes (MOR, DOR, KOR), and a non-classical nociception receptor subtype (NOR), the structures of which were recently elucidated through crystallography.[8–11]

Recent work has identified KOR as a novel promising target for pain alleviation with a lower potential of abuse than MOR.[12,13] KORs are primarily expressed in the CNS, particularly in areas of the brain that are responsible for regulating reward, mood, and cognitive functions (e.g. dysphoria and sedation). Furthermore, they participate in analgesia, respiratory depression and

dyspnea, and they can also be found in the periphery.[4,14] As a result, efforts to selectively target the KOR have been made with the goal of treating neurological disorders.[15–18] Above all, antagonists selectively targeting the KOR have been reported to be effective in the treatment of depression, psychosis, schizophrenia, addiction and anxiety.[14,19–21]

Although the classical viewpoint on GPCRs was that they function as single units, more recent evidence indicates that at least some receptors might form homo-/hetero-dimers or even oligomers. In the case of opioid receptors, there is indirect evidence that they might form dimers or higher order oligomers among themselves as well as with non-opioid receptors.[22–24] Interestingly, KOR has been reported to crystallize in a parallel homodimeric form when bound to the antagonist JDTic[10] and to the agonist MP1104,[25] however it is not clear whether this dimerization reflects a physiological organization or is an artifact caused by crystallization.[9] In addition, studies focusing on KOR heteromerization with the other OR subtypes (KOR-MOR,[26–29] KOR-DOR,[26,30,31] KOR-NOR[32]) have been conducted, the majority of which suggest the possibility of heterodimer formation. A number of bivalent ligands designed to target KOR heteromers has been synthesized.[33–38] Furthermore, two monovalent KOR heteromer-selective ligands have been reported; 6'-guanidinonaltrindole (6'-GNTI) on the KOR-DOR dimer[39] and *N*-naphthoyl-β-naltrexamine (NNTA) on the KOR-MOR dimer.[40] Still, the occurrence and functional consequences of OR oligomerization in living cells remain largely unexplored and controversial due to lack of direct methods to observe dimers and the complexity of opioid pharmacology.

The recent introduction of innovative microscopy methods to investigate GPCRs in living cells with high spatio-temporal resolution[41–44] has led to important findings on their organization, signaling and dynamics on the surface of living cells.[45–48] Within this field, the development of

novel fluorescent probes to label wild-type receptors is of high importance.[47–54] However, studies on developing KOR selective fluorescent probes have been particularly scarce. Most available probes are non-selective derivatives of wide-spectrum OR antagonists like naloxone or β-naltrexamine.[55–58] The very few high-affinity KOR fluorescent ligands available have been identified serendipitously by screening of compounds originally designed to target other OR subtypes.[59] To our knowledge, the only highly selective KOR fluorescent probes reported in the literature so far are analogues of the arylacetamide agonist ICI-199,441[60–62] and a set of fluorescent peptide probes that behave as partial agonists.[63] A KOR selective fluorescent probe with antagonistic properties, as well as a selective morphinane-based probe are currently missing. The development of such probes would be very useful to investigate the inactive state of the KOR receptor both *in vitro* and *in vivo*.

Herein, we present the synthesis, biological evaluation, and application of five fluorescent probes with high KOR affinity, based on the high affinity and selective opioid antagonist 5'-guanidinonaltrindole (5'-GNTI). After exploring their pharmacology, optical properties and dissociation kinetics, a suitable pair of these probes was used in single molecule microscopy (SMM) experiments to study spontaneous homodimerization of inactive KORs at low/physiological expression levels. Spontaneous organization of KORs in dimers, even in the non-active state, could suggest the existence of a functional unit with a potentially different pharmacologic profile than KOR monomers. Therefore, elucidating KOR homodimerization in living cells may ultimately lead to the design of new opioid drugs with higher selectivity, less side effects and more favorable pharmacological profile altogether.

5'-GNTI has been used in opioid research as a standard pharmacological tool. Its pharmacological properties have been extensively studied both *in vitro*[64–67] and *in vivo*,[68–72] as

well as its pharmacokinetic profile.[73,74] 5'-GNTI has a subnanomolar affinity for the KOR with good selectivity against MOR and DOR. Functionally, it shows low inverse agonist properties towards G protein activation.[67] Although the compound is highly water-soluble, it exhibits a slow onset and long duration of action, in addition to antidepressant-like behavioral effects and allodynia in animal models.[64,68–74] Not only have its structure-activity relationships (SARs) and binding mode been thoroughly investigated,[10,64,66,75,76] 5'-GNTI has also been successfully used as a KOR pharmacophore in the bivalent ligands KDN-21[33–35] and KMN-21[36]. These studies provide valuable insights into the optimal position for implementing a linker moiety on 5'-GNTI, without causing affinity and selectivity loss. Furthermore, information on optimal linker length and its chemical nature can also be extracted.

The selection of a suitable fluorescent dye is crucial for fluorescent ligand design. The cyanine dyes Cy5 (excitation wavelength: 647 nm) and Cy3 (excitation wavelength: 555 nm) are excellent candidates for probe design, exhibiting a non-toxic profile, pH insensitivity and photostability.[77–79] Furthermore, Cy5 has been successfully used in recently developed opioid fluorescent probes that have been successfully used both *in vitro* and *in vivo*.[47,48,59,80–82]

Results
Chemistry
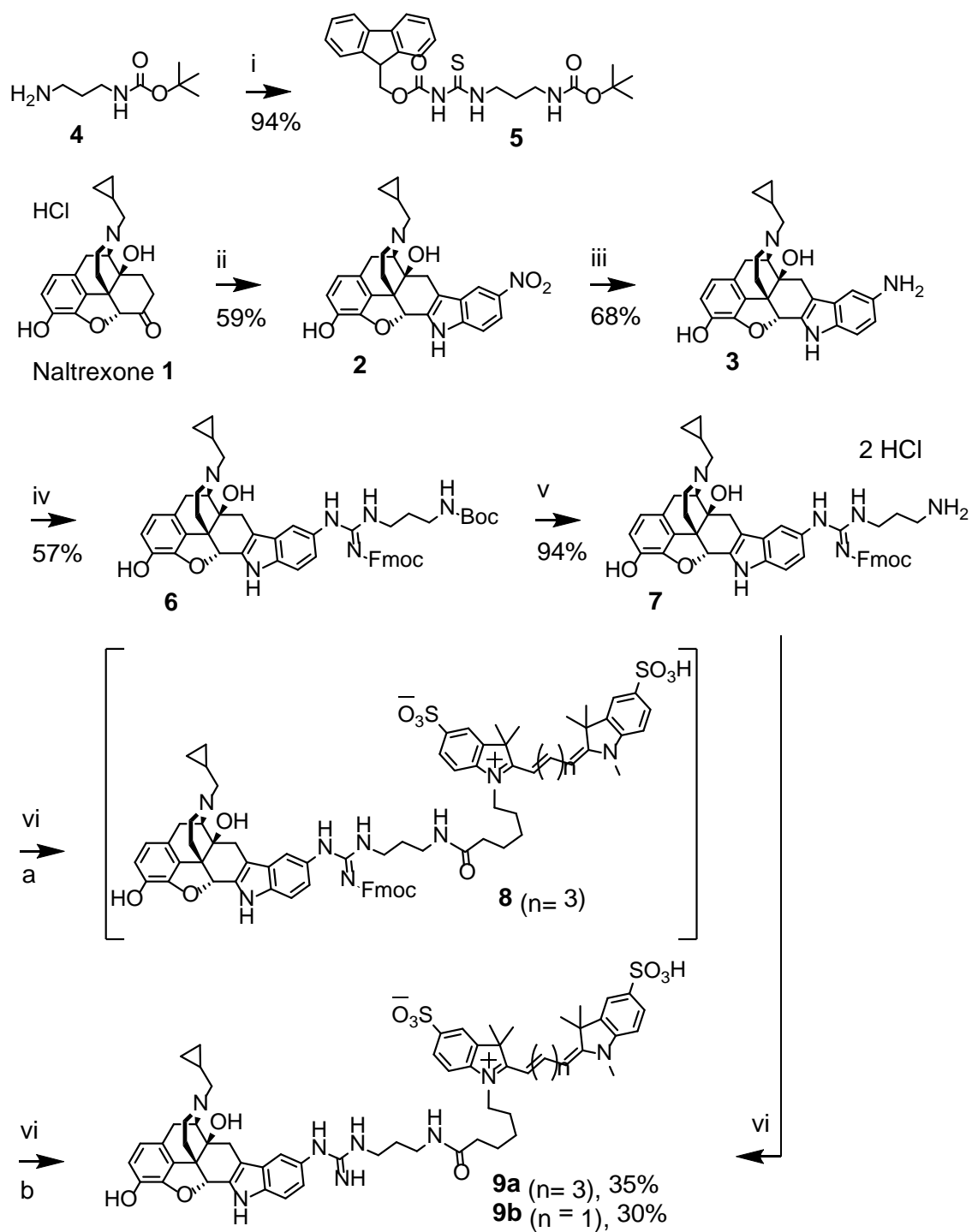
Scheme 1: Synthesis of 5'-GNTI coupled to fluorescent dyes Cy5 (**9a**) and Cy3 (**9b**), respectively, via an alkylene linker. Reaction conditions: i. Fmoc-NCS / CH$_2$Cl$_2$; ii. 4-Nitrophenylhydrazine HCl / HCl / AcOH; iii. Ra-Ni / H$_2$NNH$_2$ / EtOH; iv. **5** / HgCl$_2$ / DIPEA /

DMF; v. HCl / MeOH / EtOH; vi. a) Cy5-NHS or Cy3-NHS / DIPEA / DMF; b) Piperidine 6% / DMF

In previous studies[33–36] it had been shown that the implementation of a linker on the guanidinyl NH leads to molecules which can retain affinity, antagonistic activity and selectivity for the KOR. Inspired by these studies, and also by investigations highlighting the contribution of the linker's length and physicochemical properties in avoiding non-specific binding and preserving the pharmacological profile of the prototype ligand,[60,61,83–85] we designed three sets of fluorescent probes: a) compounds **9a** and **9b**, which bear a 11-bond aliphatic linker (Scheme 1); b) compound **13**, which bears a 17-bond linker with the incorporation of a diglycine moiety (Scheme 2); c) compounds **17a** and **17b**, which bears a 23-bond linker with the incorporation of a tetraglycine moiety (Scheme 2).
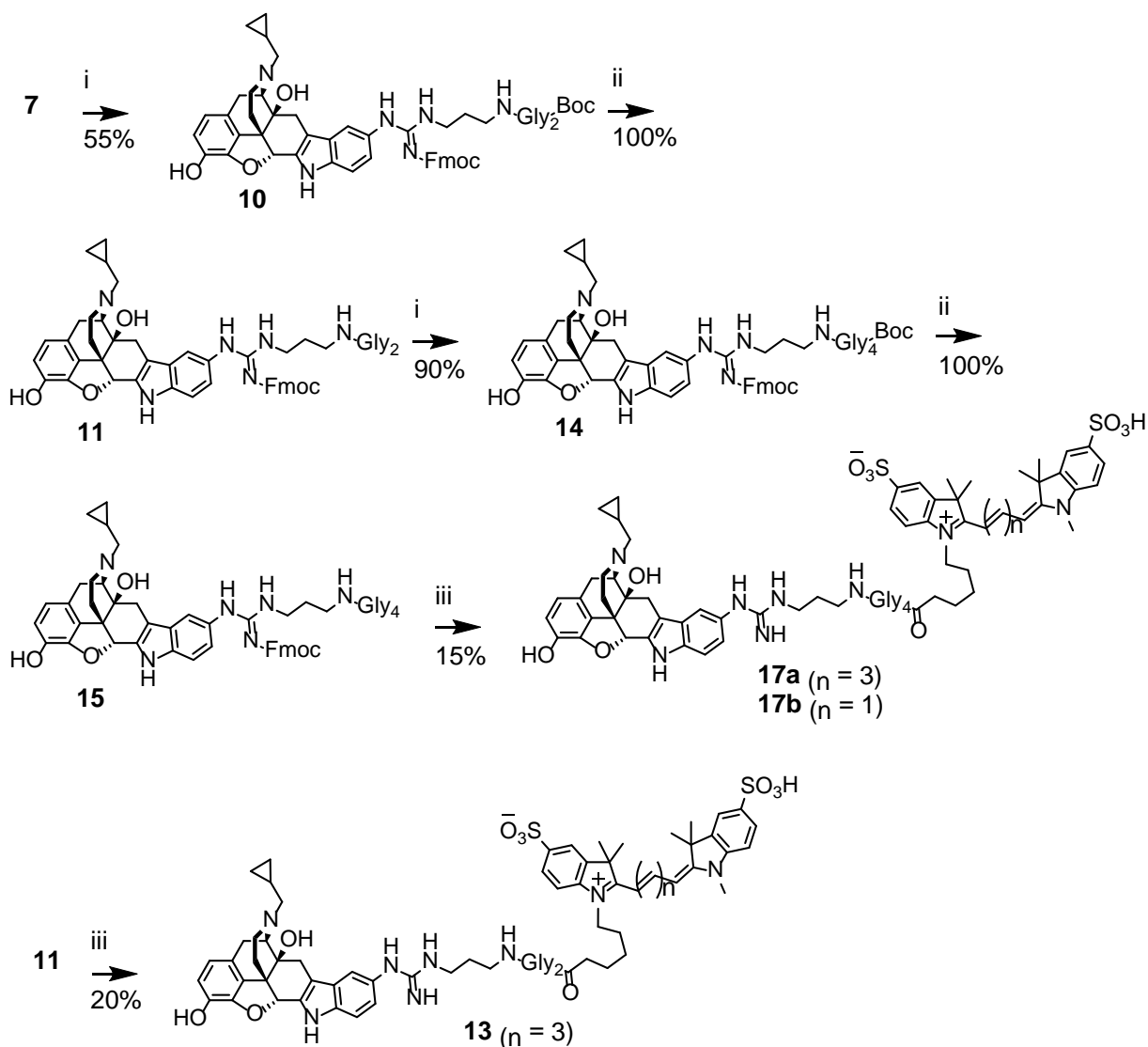
Scheme 2: Synthesis of 5'-GNTI coupled to fluorescent dyes Cy5 (**17a** and **13**) and Cy3 (**17b**), respectively, via digylcine and tetraglycine containing linkers. Reaction conditions: i. *N*-Boc-Gly$_2$ / EDCI / HOBt / DIPEA / DMF; ii. TFA 5% / CH$_2$Cl$_2$; iii. a) Cy5-NHS or Cy3-NHS / DIPEA / DMF; b) Piperidine 6% / DMF

Regarding their synthesis, an orthogonal approach was necessary in order to simultaneously accommodate the selective protection of primary amines and the protection of the guanidinyl NH throughout the synthetic scheme. Thus, Fmoc and Boc protective groups were selected for the

guanidinyl NH and the primary amines respectively. This is because the former are cleaved primarily in basic conditions (in presence of secondary amines), while the latter under acidic conditions.

5'-Nitronaltrindole **2** was synthesized from naltrexone via Fischer indole synthesis and underwent a Raney nickel catalyzed reduction to yield 5'-aminonaltrindole **3** (Scheme 1), as previously described.[66] The dual protected thiourea intermediate **5** was synthesized in quantitative yield from Fmoc-isothiocyanate and *N*-Boc-ethylenediamine **4** (Scheme 1) based on the protocol of Linton et al.[86] The diprotected guanidine compound **6** was formed using a mercury(II) chloride-assisted coupling reaction[87] (Scheme 1), based on reported protocols.[33,36,64,66] The Boc group was subsequently cleaved with an alcoholic HCl solution, and the resulting salt **7** was then coupled with Cy5 *N*-hydroxysuccinimide ester forming the Fmoc protected fluorescent ligand **8** (Scheme 1). One flask Fmoc deprotection took place by addition of piperidine (i.e. piperidine was added to the reaction mixture after completion of the coupling reaction), leading to the target compound. The purification of all target compounds was performed by reverse phase flash chromatography and reverse phase semi-preparative HPLC. For target compound **9a** in particular, purification via semi-prep RP-HPLC was performed before Fmoc cleavage, at the stage of compound **8**, as a first approach. Compound **8** was then deprotected with 6% piperidine and was purified again via semi-prep RP-HPLC. Further trialing confirmed that the deprotection step could be conducted in a one flask manner, thus this approach was favored henceforth.

Compound **7** was further used for the synthesis of the diglycine and tetraglycine analogues, after EDCI/HOBt coupling with *N*-Boc-diglycine (Scheme 2). Compound **10** underwent Boc cleavage using trifluoroacetic acid (TFA), and the salt produced (**11**) then reacted with Cy5 *N*-

hydroxysuccinimide ester towards target compound **13** after Fmoc deprotection (Scheme 2), as described above. Boc deprotection as performed in a previous stage using HCl in alcohols yielded a hydrochloric salt, which is solid and easy to handle (Scheme 1). In this stage however, the alcoholic solvent in combination with the lengthy reaction time necessary for quantitative Boc deprotection and acidic conditions caused glycine cleavage as well. Therefore, after coupling with glycine moieties, the Boc deprotection method was switched to a rapid, anhydrous TFA in dry dichloromethane protocol (Scheme 2) to avoid byproduct formation; the film-like texture of the resulting TFA salts being a minor disadvantage though.

The diglycine TFA salt intermediate **11** was coupled with *N*-Boc-diglycine forming the diprotected tetraglycine compound **14**, which is then subjected to the aforementioned synthetic steps (i.e. Boc deprotection, Cy5-NHS coupling, Fmoc deprotection) to yield target compounds **17a** and **17b** (Scheme 2). It is noteworthy to mention that intermediates **10** and **14** suffered from poor solubility in organic solvents, probably due to their high polarity. Thus, extensive workup with high volumes of chloroform/methanol mixtures was needed.

An alternative synthetic pathway was trialed for the tetraglycine compounds by reacting intermediate **7** with *N*-Cbz-tetraglycine. Due to the poor solubility of the latter, the EDCI/HOBt coupling reaction was applied in dimethyl formamide (DMF) medium as well as in pyridine medium.[88] The combination of lower yields, partial Fmoc deprotection due to the presence of pyridine, and hardship on the following Cbz deprotection rendered the latter synthetic route unfavorable though.

Pharmacology

Affinity measurements via radioligand binding were performed using membrane preparations from HEK293T cells (cf. Supporting Information). The resulting K_i values showed the

development of higher levels of KOR selectivity with incorporation of glycine moieties (Table 1); however this was not proportional to the linker length. Concentration-binding relationships at the KOR were measured also using total internal reflection fluorescence (TIRF) microscopy for compounds **9a**, **9b** and **17a** in transiently transfected CHO cells (cf. Supporting Information). The resulting K_d values were 9.5 ± 1.3 nM, 18.8 ± 13.4 nM and 4.8 ± 2.8 nM, respectively, similar to those obtained in the radioligand binding assays. All compounds exhibited very good optical properties, high signal-noise ratio and low unspecific binding.

Table 1: Radioligand binding studies

	K_i (nM) KOR	K_i (nM) DOR	K_i (nM) MOR	DOR/KOR	MOR/KOR
9b	8.6 ± 1.4	31 ± 4	380 ± 111	4	44
9a	1.4 ± 0.8	39 ± 16	40 ± 6	28	29
13	1.1 ± 0.1	106 ± 15	100 ± 34	100	91
17a	1.8 ± 0.4	193 ± 29	133 ± 14	107	74
17b	3.2 ± 0.8	280 ± 62	110 ± 14	88	34

OR subtype-specific binding affinities were measured using the radioligand [³H]diprenorphine and membrane preparations from HEK293T cells transiently transfected with MOR, DOR, KOR, respectively. Non-specific binding was determined in the presence of naloxone at a final concentration of 10 µM.

For imaging applications, fluorescent probes with slow dissociation kinetics are preferable, as this allows washing out unbound probes and retaining a high degree of labeling during imaging.

Therefore, we measured the dissociation of compounds **9a**, **13** and **17a** from KOR by TIRF microscopy. In all cases, above 90% of the probes remained bound to the receptors at the end of a 20-min wash with cell culture medium (Figure 1). This is indicative of particularly slow dissociation kinetics, which make the probes ideal for SMM and other imaging applications.
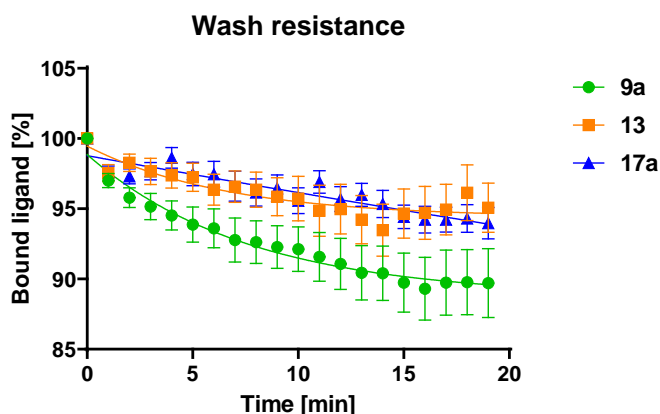
Figure 1: Normalized fluorescence intensity plotted over time and fitted with a one phase exponential decay function. Each data point is the average of three independent experiments ± S.E.M.

Intrinsic activity measurements of the probes were conducted in order to verify whether they retained the pharmacological profile of the parent compound. Receptor activation mediated by G protein signaling was determined via applying the IP-One HTRF® assay (Cisbio, Codolet, France) under co-transfection of the appropriate opioid receptor and the hybrid G protein $G\alpha_{qi}$, a $G\alpha_q$ protein with the last five C-terminal amino acids replaced by the corresponding sequence of $G\alpha_i$.[89,90] Furthermore, β-arrestin-2 recruitment was measured via the PathHunter® assay (DiscoverX, Birmingham, U.K.); in both assays, dynorphin A was used as a reference KOR agonist (cf. Supporting Information).
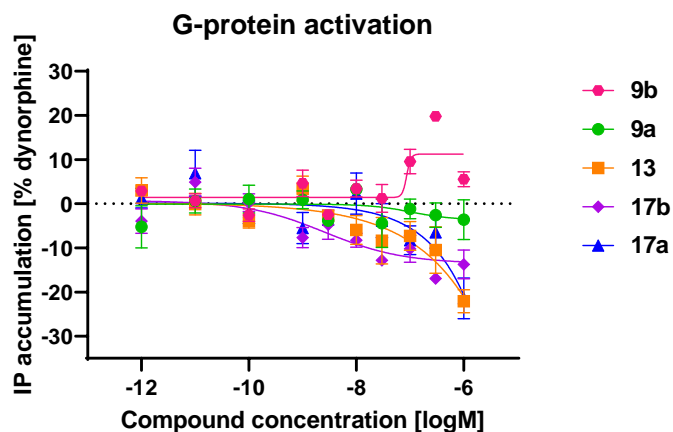
Figure 2: Accumulation of inositol monophosphate normalized to the maximum effect of dynorphine A, plotted against compound concentration ± SEM (cf. Supporting Information for single curve graphs).
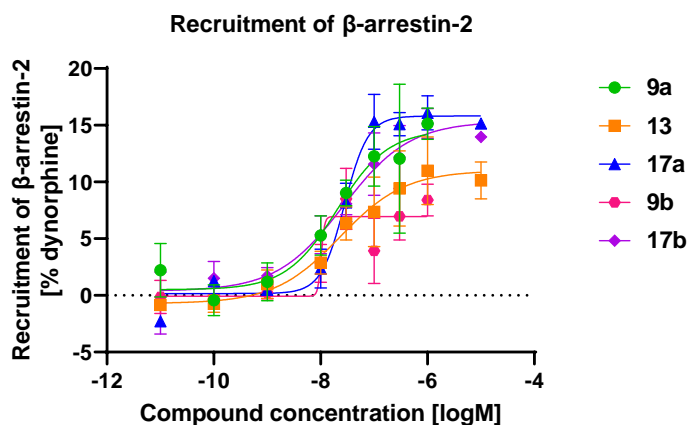
Figure 3: Recruitment of β-arrestin-2 normalized to the maximum effect of dynorphine A, plotted against compound concentration ± SEM (cf. Supporting Information for single curve graphs).

The resulting curves show that all probes apart from compounds **9a** and **9b** are very weakly inverse agonists for G protein activation (Figure 2); while all probes are very weakly partial agonist for β-arrestin-2 recruitment (Figure 3) (cf. Supporting Information).

Single Molecule Microscopy
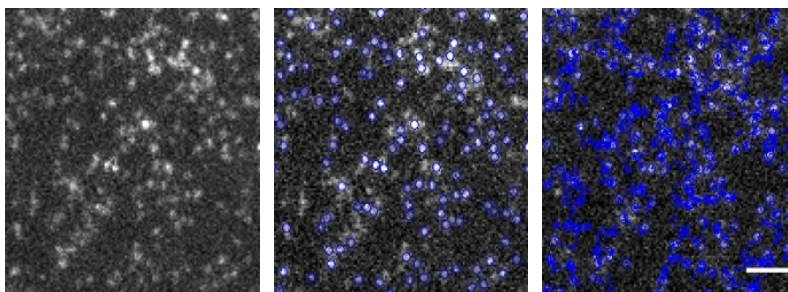
Figure 4: Single-molecule imaging of KORs labelled with **9b** in CHO cells transiently transfected with wild-type KOR and treated with 100 nM **9b** for 20 min, followed by a rapid washing step. A representative cell is shown (left). The blue circles indicate all automatically detected particles of the same cell (middle). Representative trajectories are shown (right). Scale bar: 2 μm

Fluorescent probes **9a** and **9b** were selected for SMM experiments in CHO cells transiently transfected with human KOR. This pair of probes was preferred over **17a**, **17b**, since the slightly reverse agonist profile of the latter might potentially hamper receptor oligomerization. The applied transfection protocol was designed to achieve low/physiological receptor densities on the cell surface (cf. Supporting Information). The cells were incubated with saturating concentrations of the fluorescent probes (**9a** - 10 nM; **9b** – 100 nM), rapidly washed, and immediately imaged by TIRF microscopy. The acquired movies were analysed with an automated single particle detection and tracking algorithm in MATLAB environment (Figure 4), and further investigated using custom algorithms, as previously described.[47,48,91,92]
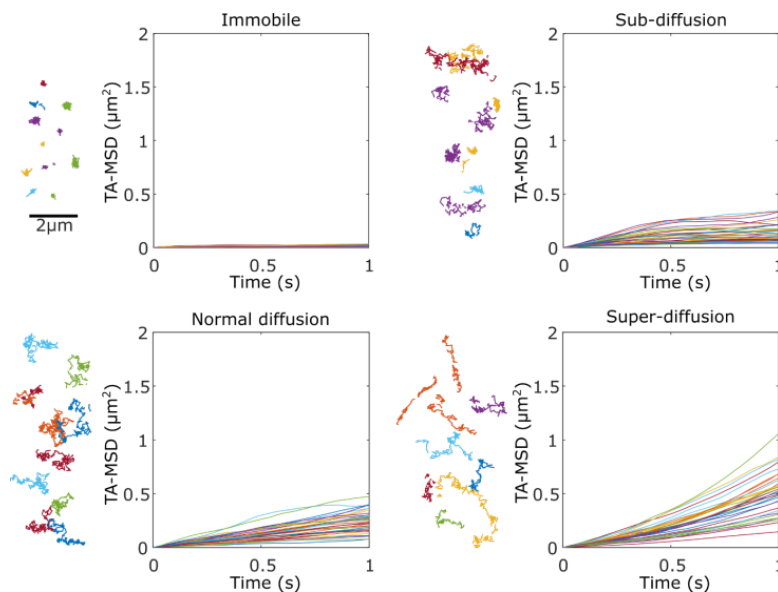
Figure 5: Representative trajectories (presented to the left) and TA-MSD vs time plots (presented to the right) of the four subtypes of motion present: immobile, sub-diffusive, diffusive and super-diffusive motion, derived from one-color SMM measurements using compound **9b**. Each plot line corresponds to the TA-MSD of a single particle over time. The trajectories of some representative particles for each motion subtype are presented on the left of the corresponding plot.
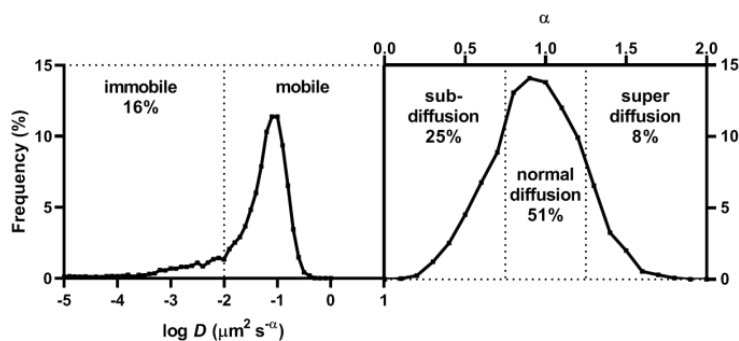
Figure 6: Distribution of labelled receptors in terms of generalized diffusion coefficient ($\log D$) and anomalous diffusion exponent (α), derived from one-color SMM measurements using compound **9b**

A time-averaged mean-squared displacement analysis (TA-MSD) was performed to characterize the movements of KOR labelled with **9b** in the cell membrane (Figure 5).[93] Single-molecule trajectories were classified into four different groups, based on both their generalized diffusion coefficient (D), and their anomalous diffusion exponent (α). The analysis (Figure 6) showed that approximately 16% of the receptors were immobile, 25% were confined (sub-diffusion), 51% followed normal Brownian diffusion, and 8% had directional motion (super-diffusion).

To investigate whether KORs form dimers at physiological expression levels, two-colour single-molecule experiments were performed. In order to estimate the frequency and duration of the receptor-receptor interactions, a control (CD86-SNAP) was introduced. CD86 is an unrelated transmembrane protein, which is not expected to interact with KOR. CD86 was labelled with silicon rhodamine (SiR) via a SNAP tag fused at its N terminus.[46–48]
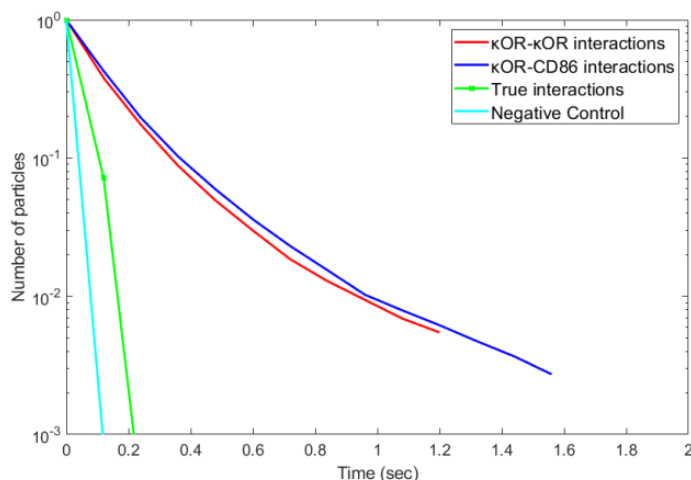
Figure 7: Deconvolved co-localisation of KOR receptors in two-colour SMM over time averaged over 34 individual cells (18 for CD86). The curve corresponding to true interactions is very close to the negative control, indicating the lack of detectable transient dimerization

First, the distribution of the co-localization times between KOR-**9a** and KOR-**9b** was measured. Then, by measuring the co-localization times between KOR-**9b** and CD86-SNAP molecules, we were able to determine the expected distribution of random co-localizations. The frequency and duration of receptor-receptor interactions were then estimated by deconvolution of the KOR-**9a** and KOR-**9b** co-localization times with those obtained with KOR-**9b** and CD86-SNAP as previously described.[47,48,92] The deconvolved co-localization times of KOR-**9a** with KOR-**9b** were virtually superimposable to those obtained with the control CD86-SNAP (Figure 7). These data suggest that KORs bound to **9a** and **9b** ligands either do not undergo significant dimerization under our experimental conditions, or the interactions are so short-lived (< 100 ms), that they cannot be detected by our method.

Discussion

The new fluorescent KOR compounds developed in this study exhibit low nanomolar affinity for the KOR (Table 1), which renders them amongst the most potent fluorescent ligands for this receptor subtype. The crucial role of linker length and composition was once more affirmed. Furthermore, the new fluorescent compounds display very good optical properties, very low unspecific binding and slow dissociation kinetics (Figure 1). As shown in the intrinsic activity assay, the compounds retain antagonistic properties (Figure 2). The SAR derived from our results (Figure 2) suggests that a shift towards G protein inverse agonism is observed with longer, peptide-extended linkers when compared to the shorter hydrocarbon linker found in compounds **9a** and **9b**. Inverse agonism was only very weak for all compounds tested, so that they essentially behave like neutral antagonists. At the same time, all the aforementioned

substitution patterns slightly promote β-arrestin-2 recruitment (Figure 3). KOR selectivity over the other ORs was observed, reaching approximately 100-fold for ligands **13** and **17a** (Table 1). The combination of all above features makes these probes valuable candidates for imaging KORs by single-molecule microscopy and other imaging methods.

Investigating potential KOR homodimerization in an inactive state at the single molecule level is relevant, because if a significant proportion of KORs on the cell surface is organized in dimers, this could have important implications for the screening and pharmacological profiling of KOR ligands. Past studies on KOR homodimerization have suggested that KOR might be constitutively organized as a dimer on the cell surface.[26,29,30] Interestingly, Ramsay et al. reported that binding to 5'-GNTI did not affect this KOR homodimeric organization.[30] However, these studies were conducted using ensemble fluorescent methods (BRET, confocal microscopy) and biochemical methods (Western blot, co-immunoprecipitation). These methods typically rely on receptor overexpression, which can artificially bring receptors in close proximity due to crowding. Furthermore, the ORs in the aforementioned studies were labelled with large protein tags (GFP, YFP, Luciferase), which were inserted in the sequences of human ORs. Although this did not affect OR functionality, the presence of large protein covalent tags might affect OR dimerization and/or trafficking.

The aforementioned studies, alongside KOR crystallization (conducted under non-physiological conditions though) and computational modelling,[94–97] suggested that KORs may have the capacity to oligomerize. However, the question remained as whether this occurs at physiological expression levels on the membrane of living cells. Using a similar SMM approach, we most recently showed that a small, but consistent fraction (4-5%) of MOR bound to a fluorescent ligand undergoes transient dimer formation lasting approximately 1-2 seconds in

low/physiological receptor density.[47,48] However, our current investigation, studying wild-type KOR expressed at low/physiological levels by single-molecule microscopy, did not detect a relevant fraction of long lasting (>100 ms) KOR dimers on the surface of living cells (Figure 7). Thus, our results do not support a model in which KOR form stable dimers that do not dissociate upon antagonist ligand binding.

Conclusion

We present herein the design, synthesis and biological testing of the first antagonistic and morphinane-based selective fluorescent probes for the KOR. These newly synthesized ligands exhibit high affinity for the KOR and excellent photophysical properties, and appear therefore ideal for advanced imaging applications, such as single-molecule microscopy. We exemplarily used probes **9a** and **9b** to study KOR kinetics, localization and homodimerization on a transfected cell line by single-molecule microscopy. These probes could be applied both *in vitro* and in native tissues to further investigate fundamental aspects of KORs such as their homo- and heteromerization. In addition, these probes could be tested against the adrenergic receptor, for which 5'-GNTI has been reported to show properties of a positive allosteric enhancer.[74]

EXPERIMENTAL SECTION

Materials & Methods

Cy3 NHS ester dye and Cy5 NHS Na^{+} ester dye were purchased from Click Chemistry Tools. Naltrexone was purchased from Carbosynth. All other chemicals and solvents were purchased from Sigma Aldrich. The thin-layer chromatography for reaction-control was performed on

coated plates (Silica Gel 60 F254). The substances were either visualized by their fluorescence, when irradiated with UV-light (256 nm), by spray-reagents (Dragendorff's reagent, Ehrlich's reagent) or by iodine coloring. Silica gel with a grain size of 0.063 - 0.2 mm (company Merck, Darmstadt, Germany) was used for the manual column chromatography. The columns were packed wet. The composition of the eluents is indicated in percentage by volume.

General Procedures

NMR spectra were recorded at room temperature on a Bruker AV 400 FT-NMR-Spectrometer (company Bruker Biospin, Karlsruhe, Germany) (^{1}H: 400 MHz, ^{13}C: 100 MHz). The residual protons and the ^{13}C-resonance signals of the deuterated solvents were used as internal standard. The chemical shifts δ were indicated in [ppm] and the coupling constants in [Hz]. The signal multiplicities were abbreviated as follows: s = singlet, d = doublet, t = triplet, q = quartet, dd = doublet of doublets, m = multiplet. Analytical HPLC was performed on a Shimadzu LC20AB system equipped with a DGU-20A3R controller, and a SPD-20A UV/Vis detector. Stationary phase was a Synergi 4u Fusion-RP (150×4.6 mm) column. Gradient MeOH/water + 0.1% formic acid (phase A/ phase B) were used as mobile phase (cf. Supporting Information for gradient system methods). For analytical HPLC a flow rate of 1 mL/min was used. ESI-MS spectral data were acquired on a Shimadzu LCMS-2020 single quadrupole LC-MS (Shimadzu Europe, Duisburg, Germany). A flash column system PuriFlash 430 by Interchim was used in the purification of the target compounds (cf. Supporting Information for gradient systems used). In cases where further purification of the target compounds was needed, it was performed via semi-preparative HPLC on the aforementioned Shimadzu system using a puri a Synergi 4u Fusion-RP 80A (250×10.0 mm) column as stationary phase and the flow rate was 2.5-3 mL/min (cf.

Supporting Information for gradient systems used). Purity of all final compounds was 95% or higher.

Synthesis

The fluorescent dyes were reacted as zwitterions. However, due to the 0.1% formic acid in the LCMS gradient system, protonation occurs also to the sulfonic acid group, leading to a +1 of the calculated mass M. Noted with #.

General method A – coupling the diglycine moieties

N-Boc-diglycine (1.1 eq) was dissolved in dry DMF under stirring and argon atmosphere. After dissolvation it was cooled to 0 °C. EDCI HCl (1.1 eq), HOBt (0.1 eq) were added. After 30 min DIPEA (2.2 eq) was added, and 5 min later the respective primary amine intermediate (1 eq). The ice bath was removed and the reaction mixture was left to slowly reach room temperature under the aforementioned conditions. After the reaction was concluded (usually 12-24h), the reaction mixture was extensively worked up with brine, chloroform and chloroform:methanol 5:1. The volume of the combined organic phases was reduced under vacuum, dried (Na_2SO_4), filtered and taken to dryness yielding a solid residue which was stored in the desiccator overnight. The crude product was purified via column chromatography.

General method B – Cleavage of *N*-Boc group from glycine moieties

The respective Boc, Fmoc diprotected intermediate was dissolved in a solution of 5% TFA in dry DCM under Ar atmosphere and stirring. The reaction was monitored with TLC, LCMS and was

concluded at ~2h. The reaction mixture was taken to dryness (rotary bath at 30°C) and stored in the desiccator. The compound was used in the next step without further purification.

General method C – coupling the precursors with the dyes

Precursor compound (1 eq) was dissolved in 1.5 mL dry DMF under stirring and argon atmosphere. After complete dissolvation, DIPEA (2.2 eq) was added and the reaction mixture was left to stir for 10 min. Cy5-NHS Na or Cy3-NHS ester (0.8 eq) was added and the reaction mixture was left to stir overnight under the aforementioned conditions with exclusion of light. After conclusion of the reaction, piperidine (90 μL – 6% v/v, Fmoc cleavage) was added in the mixture which was left to stir for 2 min and was purified via RP flash column chromatography and RP semi prep-HPLC (cf. Supporting Information for gradient methods used).

5'-Nitronaltrindole (2): 1 g (1 eq) of naltrexone HCl salt **1** (MW = 377.14) and 1.253 g (1 eq) of 4-nitrophenylhydrazine HCl salt (MW = 189.03) were dissolved in 27 mL of HCl 37% : acetic acid glacial 1:1 v/v mixture. Some desolvation problems were solved once the temperature started rising. The reaction mixture was heated at 90 °C overnight under nitrogen atmosphere and vigorous stirring. After cooling to room temperature, the reaction mixture was basified with solid Na_2CO_3, solid NaOH and saturated Na_2CO_3 solution under ice-cooling. The mixture was worked up with an extensive amount of chloroform and chloroform/isopropanol mix (4:1). The combined organic extract was filtered (paper, gravity), dried (Na_2SO_4), filtered and evaporated under reduced pressure to yield 1 g of a yellow-brown solid residue. Purification through column chromatography (DCM : MeOH : NH_3 – 40:1:0.1 → 10:1:0.1) yielded 720 mg of orange solid. Yield 59%. ^{1}H NMR (400 MHz, $CDCl_3$) δ 9.32 (s, 1H, H1'), 7.42 (s, 1H, H4'), 6.95 (s, 1H, H6'),

6.70 (dd, J = 24.9, 8.0 Hz, 2H, H1 and H2), 6.49 (s, 1H, H7'), 5.59 (s, 1H, H5), 3.41 – 3.37 (m, 1H, H9), 3.15 (d, J = 18.6 Hz, 1H, H10b), 2.90 (dd, J = 18.4, 5.6 Hz, 1H, H10a), 2.72 (d, J = 16.4 Hz, 2H, H16b and H15b), 2.54 – 2.28 (m, 5H, H15a, H16a, H8b, N-CH$_2$-CH-(CH$_2$)$_2$), 1.75 (d, J = 11.2 Hz, 1H, H8a), 1.34 – 1.16 (m, 1H, N-CH$_2$-CH-(CH$_2$)$_2$), 0.95 – 0.78 (m, 1H, N-CH$_2$-CH-(CH$_2$)$_2$), 0.58 (d, J = 7.7 Hz, 2H, N-CH$_2$-CH-(CH$_2$)$_2$), 0.17 (d, J = 4.2 Hz, 2H, N-CH$_2$-CH-(CH$_2$)$_2$). ^{13}C NMR (100 MHz, CDCl$_3$) δ 120.04 (C1), 117.89 (C2), 117.55 (C6'), 115.39 (C4'), 110.36 (C7'), 84.87 (C5), 62.33 (C9), 59.60 (N-CH$_2$-CH-(CH$_2$)$_2$), 48.26, 43.61 (C16), 31.55 (C8), 28.14 (C15), 23.29 (C10), 9.51 (N-CH$_2$-CH-(CH$_2$)$_2$), 4.08 (2C, N-CH$_2$-CH-(CH$_2$)$_2$). MS: C$_{26}$H$_{25}$N$_3$O$_5$ calc. 459.18. ESI (m/z): 460.15 [M+H]$^+$

5'-Aminonaltrindole (3): 5'-nitronaltrindole **2** (392 mg, 1 eq) was well dissolved in 12 mL of ethanol under stirring. An amount of wet Ra-Ni was brought into a small penicillin type vial containing fresh deionized water, so as to wash out acid which may form during its storage. From there the wet solid was later added in the reaction mixture. Four teaspoons of wet Ra-Ni were added. Hydrazine (240 μL, 7.7 eq) was added carefully in the reaction mixture which was left to stir at room temperature under nitrogen atmosphere (balloon). After 6h the reaction was concluded. The reaction mixture was filtered in celite pad and the cake was thoroughly washed with ethanol, methanol and boiling methanol. The combined organic fractions of the filtrate were reduced under vacuum, dried (Na$_2$SO$_4$), filtered and taken to dryness. The crude product remained in the desiccator for 48h yielding 383 mg of crude product as a pale yellow solid powder. Purification via column (20:1:0.1 → 17:1:0.1; DCM:MeOH:NH$_3$) affording 249 mg of product. Yield: 68%. ^{1}H NMR (400 MHz, MeOD) δ 7.11 (dd, J = 8.5, 0.5 Hz, 1H, H7'), 6.82 – 6.75 (m, 1H, H4'), 6.66 (dd, J = 8.5, 2.2 Hz, 1H, H6'), 6.54 (q, J = 8.1 Hz, 2H, H1 and H2), 5.55

(s, 1H, H5), 3.40 – 3.33 (m, 1H, H9), 3.16 (d, J = 18.6 Hz, 1H, H10b), 2.81 (dd, J = 18.6, 6.6 Hz, 1H, H10a), 2.76 – 2.68 (m, 2H, H15b and H16b), 2.55 (dd, J = 15.7, 0.9 Hz, 1H, H15a), 2.44 (dd, J = 6.6, 1.9 Hz, 2H, N-$\underline{CH_2}$-CH-(CH$_2$)$_2$), 2.38 – 2.24 (m, 2H, H8b and H16a), 1.76 – 1.62 (m, 1H, H8a), 1.41 – 1.23 (m, 1H, H15b), 1.03 – 0.82 (m, 2H, H15a and N-CH$_2$-$\underline{CH}$-(CH$_2$)$_2$), 0.65 – 0.47 (m, 2H, N-CH$_2$-CH-$\underline{(CH_2)_2}$), 0.28 – 0.07 (m, 2H, N-CH$_2$-CH-$\underline{(CH_2)_2}$). ^{13}C NMR (100 MHz, MeOD) δ 119.68 (C1), 118.31 (C2), 115.16 (C6'), 112.60 (C7'), 105.76 (C4'), 86.27 (C5), 63.57 (C9), 60.41 (N-$\underline{CH_2}$-CH-(CH$_2$)$_2$), 44.96 (C16), 32.68 (C8), 29.86 (C15), 24.09 (C10), 10.17 (N-CH$_2$-$\underline{CH}$-(CH$_2$)$_2$), 4.63 (N-CH$_2$-CH-$\underline{(CH_2)_2}$), 4.09 (N-CH$_2$-CH-$\underline{(CH_2)_2}$). MS: C$_{26}$H$_{27}$N$_3$O$_3$ calc. 429.21. ESI (m/z): 430.15 [M+H]$^+$

(9'H-fluoren-9'-yl)methyl (1-((3-((($tert$-butoxy)oxo)amino)propyl)amino)thioxo)carbamate (5): N-Boc-1,3-propandiamine **4** (244 mg, 1 eq) was dissolved in 5 mL dry DCM under nitrogen atmosphere (balloon) and stirring. The reaction mixture was then ice-cooled to 0 °C and 9H-fluoren-9-ylmethoxycarbonyl isothiocyanate (434 mg, 1.1 eq) was added. The reaction mixture was left to stir under nitrogen and slowly come to room temperature. After 5h TLC control (3:1, petrol ether:ethyl acetate, Rf = 0.6) showed that the reaction was concluded. An approximately double amount of pentane was added to the reaction mixture under stirring, leading to the formation of a fine white precipitate (solid with a paper-like texture), which was filtered off and dried in the desiccator. 666 mg – quantitative. ^{1}H NMR (400 MHz, CDCl$_3$) δ 8.07 (s, 1H, NH), 7.78 (d, J = 7.6 Hz, 2H, H4' and H5'), 7.55 (dd, J = 7.5, 0.8 Hz, 2H, H1' and H8'), 7.43 (t, J = 7.3 Hz, 2H, H3' and H6'), 7.33 (td, J = 7.5, 1.1 Hz, 2H, H2' and H7'), 4.84 (s, 1H, NH), 4.50 (d, J = 6.7 Hz, 2H, H10'), 4.23 (t, J = 6.7 Hz, 1H, H9'), 3.74 (q, J = 6.6 Hz, 2H, H3), 3.19 (d, J = 6.1 Hz, 2H, H5), 1.83 (p, J = 6.6 Hz, 2H, H4), 1.44 (s, 9H, H8-H10). ^{13}C NMR (100 MHz,

CDCl$_3$) δ 128.25 (2C, C2' and C7'), 127.42 (2C, C3' and C6'), 124.96 (2C, C4' and C5'),

120.38 (2C, C1' and C8'), 68.36 (1C, C10'), 46.69 (1C, C9'), 42.92 (1C, C3), 37.64 (1C, C5),

29.31 (1C, C4), 28.55 (3C, C8-C10). MS: C$_{24}$H$_{29}$N$_3$O$_4$S calc. 455.19. ESI (m/z): 456.19 [M+H]$^+$,

478.10 [M+Na]$^+$, 933.10 [2M+Na]$^+$

_ter_t-butyl (3-((_E_)-2-(1-((9_H_-fluoren-9-yl)methoxy)oxo)-3-(5'-guanidinonaltrindole)propyl)carbamate (6): 5'-aminonaltrindole **3** (235 mg, 1 eq) was

dissolved in 2 mL of dry DMF under stirring and nitrogen atmosphere (balloon). After full

dissolution the reaction mixture was cooled to 0 ºC (ice-bath). When the reaction mixture was

cooled down, DIPEA (205 μL, 2.2 eq) and intermediate **5** (275 mg, 1.1 eq) were added. The

reaction mixture was left to stir under ice-bath cooling and nitrogen atmosphere until everything

was nicely dissolved; the mixture retains a dark red color. HgCl$_2$ (164 mg, 1.1 eq) was added in

one portion and rapid stirring was maintained for 20 min under ice cooling and nitrogen

atmosphere. Afterwards the ice-bath was removed and the reaction mixture was left to slowly

reach room temperature. After 2h the color changed to black-brown and the reaction mixture had

become quite viscous (indication of extended HgS formation). TLC control (15:1:0.1 –

DCM:MeOH:NH$_3$) confirmed that the reaction was concluded. An amount of methanol was

added, and the mixture was filtered through a celite pad to remove HgS. The cake was

subsequently washed with pure methanol and boiling methanol. The filtrate volume was reduced

under vacuum, dried (Na$_2$SO$_4$), filtered and taken to dryness under reduced pressure to afford

629 mg of dark-brown solid crude product. Trialing (2D TLC, incubation, incubation at 40ºC)

showed that the compound is stable in DCM:MeOH:NH$_3$ environment. Purified via column

chromatography (30:1:0.1 → 20:1:0.1 – DCM:MeOH:NH$_3$) yielding 264 mg of light pink solid.

Yield: 57%. ^{1}H NMR (400 MHz, CDCl$_3$) δ 10.34 (s, 1H, NH), 9.18 (s, 1H, NH), 7.81 – 7.64 (m, 3H, H6' and H4'' and H5''), 7.36 (t, J = 7.4 Hz, 2H, H3'' and H6''), 7.30 – 7.27 (m, 2H, H1'' and H8''), 7.09 (d, J = 15.1 Hz, 1H, H7'), 6.69 (d, J = 20.8 Hz, 1H, H4'), 6.63 (d, J = 8.0 Hz, 1H, H2), 6.51 (d, J = 8.1 Hz, 1H, H1), 5.60 (s, 1H, H5), 4.33 (br s, 2H, H10''), 3.36 (d, J = 13.9 Hz, 3H, H1''' and H9''), 3.04 (dd, J = 38.8, 12.0 Hz, 2H, H3'''), 2.75 (dd, J = 34.4, 11.7 Hz, 2H, H10a, NH), 2.55 (d, J = 15.6 Hz, 1H, H10b), 2.32 (dd, J = 47.6, 17.8 Hz, 4H, H2''' and N-CH$_2$-CH-(CH$_2$)$_2$), 1.93 (s, 1H, H8a), 1.44 (d, J = 5.2 Hz, 2H, H8b, H16b), 1.31 (s, 9H, H4'''-H6'''), 1.26 (s, 3H, H16a, H9, OH), 1.17 – 1.11 (m, 1H, H15b), 0.93 – 0.78 (m, 2H, H15a and N-CH$_2$-CH-(CH$_2$)$_2$), 0.55 (d, J = 7.2 Hz, 2H, N-CH$_2$-CH-(CH$_2$)$_2$), 0.15 (d, J = 3.9 Hz, 2H, N-CH$_2$-CH-(CH$_2$)$_2$). ^{13}C NMR (100 MHz, CDCl$_3$) δ 127.62 (2C, C3'' and C6''), 127.18 (2C, C1'' and C8''), 125.69 (2C, C6' and C7'), 119.92 (2C, C4'' and C5''), 119.20 (2C, C1 and C2), 117.46 (1C, C4'), 84.98 (1C, C5), 67.67 (1C, C10''), 62.39 (2C, C1''' and C3'''), 59.55 (N-CH$_2$-CH-(CH$_2$)$_2$), 47.28 (1C, C9''), 30.45 (1C, C16), 29.86 (1C, C15), 28.83 1C, C10), 28.50 (3C, C4'''-C6'''), 23.30 (1C, N-CH$_2$-CH-(CH$_2$)$_2$), 22.61 (1C, C8), 3.97 (2C, N-CH$_2$-CH-(CH$_2$)$_2$). MS: C$_{50}$H$_{54}$N$_6$O$_7$ calc. 850.41. ESI (m/z): 426.45 [M+2H]$^{2+}$, 851.41 [M+H]$^+$

(*E*)-2-(1-((9*H*-fluoren-9-yl)methoxy)oxo)-1-(3-aminopropyl)-3-(5'-guanidinonaltrindole) (7): Intermediate **6** (58 mg, 1 eq) was dissolved in 1 mL of dry ethanol and cooled to 0 °C under stirring and argon atmosphere (balloon). HCl in methanol 1.25 M (3.4 mL, 44 eq) was added dropwise and the reaction mixture was left to stir under argon atmosphere without renewing the ice-bath, so that it slowly reaches room temperature. After two overnights the product was formed quantitatively and the reaction mixture was taken to dryness affording a pale white solid (59 mg). ^{1}H NMR (400 MHz, MeOD) δ 7.72 (d, J = 7.1 Hz, 2H, H4'' and H5''), 7.54 (ddd, J =

22.2, 13.3, 5.9 Hz, 2H, H3'' and H6''), 7.42 (t, J = 8.9 Hz, 2H, H1'' and H8''), 7.38 – 7.25 (m, 2H, H2'' and H7''), 7.24 (dd, J = 14.5, 7.2 Hz, 2H, H6' and H7'), 6.98 (d, J = 8.6 Hz, 1H, H4'), 6.66 – 6.54 (m, 2H, H1 and H2), 5.70 (s, 1H, H5), 4.51 (d, J = 18.7 Hz, 2H, H10''), 4.22 (br s, 1H, H9''), 3.61 – 3.28 (m, 5H, H1''', NH_3^+), 3.17 (dd, J = 12.5, 3.9 Hz, 1H, H10a), 3.09 – 2.82 (m, 2H, H3'''), 2.79 – 2.62 (m, 3H, H10b, H9, H8b), 1.95 (dd, J = 27.7, 14.2 Hz, 4H, H2''', N-$\underline{CH_2}$-CH-$(CH_2)_2$), 1.23 (s, 2H, H16a and H8a), 1.17 – 1.04 (m, 2H, H15a and N-CH$_2$-$\underline{CH}$-$(CH_2)_2$), 0.81 (dd, J = 23.0, 20.2 Hz, 4H, H15b, H16b and N-CH$_2$-CH-$\underline{(CH_2)_2}$), 0.50 (s, 2H, N-CH$_2$-CH-$\underline{(CH_2)_2}$). ^{13}C NMR (101 MHz, MeOD) δ 129.24 (2C, C2'' and C7''), 128.45 (2C, C3'' and C6''), 126.19 (2C, C4'' and C5''), 121.25 (2C, C6' and C7'), 120.83 (1C, C4'), 120.71 (1C, C2), 119.55 (1C, C1), 84.97 (1C, C5), 69.92 (1C, C10''), 63.74 (1C, C9), 59.10 (1C, N-$\underline{CH_2}$-CH-$(CH_2)_2$), 47.99 (1C, C9''), 47.78 (1C, C16), 29.91 (1C, C2'''), 25.24 (1C, C15), 7.06 (1C, C10), 6.46 (1C, N-CH$_2$-$\underline{CH}$-$(CH_2)_2$), 3.59 (2C, N-CH$_2$-CH-$\underline{(CH_2)_2}$). Purity: 95%. MS: $C_{45}H_{46}N_6O_5$ calc. 750.35. ESI (m/z): 376.35 $[M+2H]^{2+}$, 751.40 $[M+H]^+$

1-((*E*)-5-((((4b*S*,8*R*,8a*S*,14b*R*)-7-(cyclopropylmethyl)-1,8a-dihydroxy-5,6,7,8,8a,9,14,14b-octahydro-4,8-methanobenzofuro[2,3-a]pyrido[4,3-b]carbazol-11-yl)amino)-1-(9*H*-fluoren-9-yl)-3,11-dioxo-2-oxa-4,6,10-triazahexadec-4-en-16-yl)-3,3-dimethyl-2-((1*E*,3*E*)-5-((*E*)-1,3,3-trimethyl-5-sulfoindolin-2-ylidene)penta-1,3-dien-1-yl)-3*H*-indol-1-ium-5-sulfonate (**8**): As a first approach, the Fmoc protected probe **8** was purified, then deprotected and purified again to reach target compound **9a**. The reaction mixture was taken to dryness using the oil pump with liquid nitrogen. The crude product was purified via RP semi-prep HPLC (cf. Supporting Information for gradient system method; flow rate 3 mL/min). Purity: 96%. MS: calc. 1374.55. ESI (m/z): 1376.20 $[M+1+H]^+$, 688.60 $[M+1+2H]^{2+}$ #

1-(6-((3-(3-((4bS,8R,8aS,14bR)-7-(cyclopropylmethyl)-1,8a-dihydroxy-5,6,7,8,8a,9,14,14b-octahydro-4,8-methanobenzofuro[2,3-a]pyrido[4,3-b]carbazol-11-yl)guanidino)propyl)amino)-6-oxohexyl)-3,3-dimethyl-2-((1E,3E)-5-((E)-1,3,3-trimethyl-5-sulfoindolin-2-ylidene)penta-1,3-dien-1-yl)-3H-indol-1-ium-5-sulfonate (9a): The pure **8** was treated with 1 mL of 6% piperidine in DMF under stirring for 2 min and then taken to dryness using the oil pump and liquid N_2. LCMS control verified total Fmoc deprotection, the product peak and the 1-((9H-fluoren-9-yl)methyl)piperidine peak. Amount: 7.3 mg. Yield: 35%. Purity: 96%. MS: calc. 1152.48. ESI (m/z): 577.45 [M+1+2H]$^{2+}$ [#]

1-(6-((3-(3-((4bS,8R,8aS,14bR)-7-(cyclopropylmethyl)-1,8a-dihydroxy-5,6,7,8,8a,9,14,14b-octahydro-4,8-methanobenzofuro[2,3-a]pyrido[4,3-b]carbazol-11-yl)guanidino)propyl)amino)-6-oxohexyl)-3,3-dimethyl-2-((E)-3-((E)-1,3,3-trimethyl-5-sulfoindolin-2-ylidene)prop-1-en-1-yl)-3H-indol-1-ium-5-sulfonate (9b): Application of General method C. Amount: 5.4 mg. Yield: 30%. Purity: 99%. MS: $C_{60}H_{70}N_8O_{10}S_2$ calc. 1126.47. ESI (m/z): 1128.00 [M+1+H]$^+$, 564.50 [M+1+2H]$^{2+}$ [#]

***tert*-butyl (2-((2-((3-(3-((1-((9H-fluoren-9-yl)methoxy)oxo)-3-(5'-guanidinonaltrindole)propyl)amino)-2-oxoethyl)amino)-2-oxoethyl)carbamate (10):**
Application of General method A, yielding 268 mg of a residue which was stored in the desiccator overnight. The crude product was purified via column chromatography (20:1:0.1 → 15:1:0.1 – DCM:MeOH:NH$_3$) affording 105 mg of yellow-white powder. Yield: 60%. ^{1}H NMR (400 MHz, CDCl$_3$) δ 7.69 (dd, *J* = 28.2, 6.8 Hz, 3H, H6', H4'' and H5''), 7.36 (m, 2H, H3'' and

H6''), 7.29 (m, 2H, H1'' and H8''), 7.10 (m, 2H, H7' and 1'-NH), 6.79 (m, 1H, H4'), 6.62 (s, 1H, H2), 6.51 (s, 1H, H1), 5.62 (s, 1H, H5), 5.37 (m, 2H, H4'''), 4.52 (s, 2H, H10''), 4.29 (m, 2H, H5'''), 3.46 (m, 3H, H1''' and NH), 3.37 (s, 1H, H9''), 3.09 (d, J = 17.8 Hz, 2H, H3'''), 2.81 (dd, J = 22.5, 8.8 Hz, 3H, H10a, H9, NH), 2.27 (m, 5H, H2''' and N-$\underline{CH_2}$-CH-(CH$_2$)$_2$), 2.02 (m, 1H, H8a), 1.39 (s, 9H, H6'''-H8'''), 1.24 (m, 5H, H15b, H16, H8b), 0.82 (m, 4H, H15a, NH, NH and N-CH$_2$-$\underline{CH}$-(CH$_2$)$_2$), 0.54 (br s, 2H, N-CH$_2$-CH-$\underline{(CH_2)_2}$), 0.14 (br s, 2H, N-CH$_2$-CH-$\underline{(CH_2)_2}$). ^{13}C NMR (101 MHz, CDCl$_3$) δ 127.77 (2C, C3'' and C6''), 127.22 (2C, C1'' and C8''), 125.22 (2C, C6' and C7'), 120.11 (2C, C4'' and C5''), 119.24 (2C, C1 and C2), 116.51 (1C, C4'), 85.17 (1C, C5), 66.56 (1C, C10''), 63.80 (1C, C3'''), 60.98 (1C, C2'''), 59.91 (N-$\underline{CH_2}$-CH-(CH$_2$)$_2$), 47.36 (1C, C9''), 44.71 (1C, C5'''), 43.76 (1C, C4'''), 29.83 (1C, C15), 29.40 (1C, C10), 28.47 (3C, C6'''-C8'''), 23.16 (1C, N-CH$_2$-$\underline{CH}$-(CH$_2$)$_2$), 22.85 (1C, C8), 5.76 (2C, N-CH$_2$-CH-$\underline{(CH_2)_2}$). MS: C$_{54}$H$_{60}$N$_8$O$_9$ calc. 964.45. ESI (m/z): 965.50 [M+H]$^+$, 483.45 [M+2H]$^{2+}$

***N*-(3-((*E*)-2-(1-((9*H*-fluoren-9-yl)methoxy)oxo)-3-(5'-guanidinonaltrindole)propyl)-2-(2-aminoacetamido)acetamide (11):** Application of General method B. 25 mg of salt (quantitative). Purity: 93%. MS: C$_{49}$H$_{52}$N$_8$O$_7$ calc. 864.40. ESI (m/z): 865.40 [M+H]$^+$, 433.35 [M+2H]$^{2+}$

1-(1-((((4b*S*,8*R*,8a*S*,14b*R*)-7-(cyclopropylmethyl)-1,8a-dihydroxy-5,6,7,8,8a,9,14,14b-octahydro-4,8-methanobenzofuro[2,3-a]pyrido[4,3-b]carbazol-11-yl)amino)-1-imino-7,10,13-trioxo-2,6,9,12-tetraazaoctadecan-18-yl)-3,3-dimethyl-2-((1*E*,3*E*)-5-((*E*)-1,3,3-trimethyl-5-sulfoindolin-2-ylidene)penta-1,3-dien-1-yl)-3*H*-indol-1-ium-5-sulfonate (13):

Application of General method C. Amount: 4.5 mg. Yield: 20%. Purity: 97%. MS: $C_{66}H_{78}N_{10}O_{12}S_2$ calc. 1266.52. ESI (m/z): 634.45 $[M+1+2H]^{2+}$ [#]

tert-butyl ((_E_)-5-((5'-aminonaltrindole)-1-(9_H_-fluoren-9-yl)-3-oxo-11,14,17,20-tetraoxo-2-oxa-4,6,10,13,16,19-hexaazahenicos-4-en-21-yl)carbamate (14): Application of General method A, yielding 100 mg of a residue which was stored in the desiccator overnight. The crude product was purified via column chromatography (15:1:0.1 → 10:1:0.1 – DCM:MeOH:NH₃) affording 48 mg of yellow-white powder. Yield: 95%. ^{1}H NMR (400 MHz, MeOD) δ 7.78 (ddd, J = 7.4, 2.0, 1.2 Hz, 3H, H6', H4'' and H5''), 7.71 (m, 2H, H2'' and H7''), 7.37 (m, 3H, H3'', H6'', H4'), 7.30 (m, 2H, H1'' and H8'') 6.94 (d, J = 8.3 Hz, 1H, H7') , 6.61 (s, 2H, H1 and H2), 6.13 (s, 1H, 1'-NH), 5.66 (s, 1H, H5), 4.41 (dd, J = 9.0, 3.7 Hz, 2H, H10''), 4.30 (m, 1H, H9''), 3.80 (d, J = 7.2 Hz, 2H, H7'''), 3.71 (m, 6H, H4'''-H6'''), 3.63 (s, 1H, NH), 3.60 (s, 2H, H1'''), 3.27 (m, 3H, H3''', NH), 3.17 (m, 3H, H2''' and NH), 2.62 (s, 2H, H9 and H10a), 1.42 (s, 9H, H8'''-H10'''), 1.37 (s, 2H, H10b, NH), 1.35 (s, 2H, H8b, NH), 1.29 (m, 6H, H16b, H8a, N-CH₂-CH-(CH₂)₂, NH, OH), 1.09 (t, J = 7.2 Hz, 2H, H15b, H16a), 0.89 (m, 6H, H15a, NH, N-CH₂-CH-(CH₂)₂ and N-CH₂-CH-(CH₂)₂), 0.37 (s, 1H, N-CH₂-CH-(CH₂)₂). ^{13}C NMR (101 MHz, MeOD) δ 130.01 (1C, C4'), 128.86 (2C, C2'' and C7''), 128.27 (2C, C3'' and C6''), 126.42 (2C, C4'' and C5''), 122.68 (1C, C1), 122.18 (1C, C2), 121.07 (2C, C1'' and C8''), 120.81 (1C, C6'), 120.45 (1C, C7'), 85.54 (1C, C5), 68.58 (1C, C10''), 64.45 (1C, C1'''), 63.76 (1C, C3'''), 57.20 (N-CH₂-CH-(CH₂)₂), 49.42 (1C, C7'''), 49.21 (1C, C9''), 48.71 (1C, C9), 44.95 (1C, C6'''), 44.25 (1C, C15), 44.06 (1C, C5'''), 43.75 (1C, C4'''), 30.87 (1C, C8), 30.46 (1C, C16), 30.14 (1C, C10), 28.85 (3C, C8'''-C10'''), 23.87 (1C, N-CH₂-CH-(CH₂)₂), 3.90 (2C, N-CH₂-CH-(CH₂)₂). MS: $C_{58}H_{66}N_{10}O_{11}$ calc. 1078.49. ESI (m/z): 1079.20 $[M+H]^+$, 540.40 $[M+2H]^{2+}$.

N-(3-((E)-2-(1-((9H-fluoren-9-yl)methoxy)oxo)-3-(5'-guanidinonaltrindole)propyl)-2-(2-(2-(2-aminoacetamido)acetamido)acetamido)acetamide (15): Application of General method B. 55 mg of salt (quantitative). Purity: 73%. MS: $C_{53}H_{58}N_{10}O_9$ calc. 978.44. ESI (m/z): 979.20 [M+H]$^+$, 490.25 [M+2H]$^{2+}$, 327.20 [M+3H]$^{3+}$

1-(1-(((4bS,8R,8aS,14bR)-7-(cyclopropylmethyl)-1,8a-dihydroxy-5,6,7,8,8a,9,14,14b-octahydro-4,8-methanobenzofuro[2,3-a]pyrido[4,3-b]carbazol-11-yl)amino)-1-imino-7,10,13,16,19-pentaoxo-2,6,9,12,15,18-hexaazatetracosan-24-yl)-3,3-dimethyl-2-((1E,3E)-5-((E)-1,3,3-trimethyl-5-sulfoindolin-2-ylidene)penta-1,3-dien-1-yl)-3H-indol-1-ium-5-sulfonate (17a): Application of General method C. Amount: 3.7 mg. Yield: 15%. Purity: 99%. MS: $C_{70}H_{84}N_{12}O_{14}S_2$ calc. 1380.57. ESI (m/z): 691.50 [M+1+2H]$^{2+}$ [#]

1-(1-(((4bS,8R,8aS,14bR)-7-(cyclopropylmethyl)-1,8a-dihydroxy-5,6,7,8,8a,9,14,14b-octahydro-4,8-methanobenzofuro[2,3-a]pyrido[4,3-b]carbazol-11-yl)amino)-1-imino-7,10,13,16,19-pentaoxo-2,6,9,12,15,18-hexaazatetracosan-24-yl)-3,3-dimethyl-2-((E)-3-((E)-1,3,3-trimethyl-5-sulfoindolin-2-ylidene)prop-1-en-1-yl)-3H-indol-1-ium-5-sulfonate (17b): Application of General method C. Amount: 2.8 mg. Yield: 15%. Purity: 99%. MS: $C_{68}H_{82}N_{12}O_{14}S_2$ calc. 1354.55. ESI (m/z): 678.45 [M+1+2H]$^{2+}$ [#]

Pharmacology assays

Radioligand binding studies: Binding affinities towards the human DOR, KOR and MOR were determined as described previously.[98,99] In brief, membranes were prepared from HEK293T

cells each transiently transfected with the cDNAs for DOR, KOR (both cDNAs obtained from the cDNA resource center, www.cdna.org) and MOR, respectively (generous gift from the Ernest Gallo Clinic and Research Center, UCSF, CA). Receptor densities (B_{max} value) and specific binding affinities (K_D value) for the radioligand [³H]diprenorphine (specific activity 31 Ci/mmol, PerkinElmer, Rodgau, Germany) were determined to be 1,700 fmol/mg protein, 0.25 nM for DOR, 6,500 fmol/mg protein, 0.13 nM for KOR, and 1,400±780 fmol/mg protein, 0.078±0.002 nM for MOR, respectively. Competition binding experiments were performed by incubating membranes in binding buffer (50 mM Tris, 5 mM $MgCl_2$, 0.1 mM EDTA, 5 µg/mL bacitracin and 5 µg/mL soybean trypsin inhibitor at pH 7.4) at a final protein concentration of 2-14 µg/well, together with the radioligand (final concentration 0.3 nM for DOR, KOR, 0.2-0.3 nM for MOR) and varying concentrations of the competing ligands for 60 minutes at 37 °C. Non-specific binding was determined in the presence of naloxone at a final concentration of 10 µM. The protein concentration was established using the method of Lowry.[100] The resulting competition curves were analyzed by nonlinear regression using the algorithms implemented in PRISM 6.0 (GraphPad Software, San Diego, CA) to provide an IC_{50} value, which was subsequently transformed into the K_i value employing the equation of Cheng and Prusoff.[101]

Accumulation of inositol mono phosphate (IP) as functional assay for G-protein mediated signaling: Determination of the activation of DOR, KOR and MOR was measured applying the IP-One HTRF® assay (Cisbio, Codolet, France) according to the manufacturer's protocol and as described previously.[90] In brief, HEK-293T cells were grown to a confluence of approx. 70% and transiently co-transfected with the cDNA of the human KOR (cDNA Resource Center, Bloomsberg, PA) and of the hybrid G-protein Gα$_{qi}$ (Gα$_q$ protein with the last five amino acids at the C-terminus replaced by the corresponding sequence of Gα$_i$; gift from The J. David Gladstone

Institutes, San Francisco, CA)[89] applying the Mirus TransIT-293 transfection reagent (Peqlab, Erlangen, Germany). After one day cells were detached from the culture dish with Versene (Life Technologies, Darmstadt, Germany), seeded into black 384-well plates (10000 cells/well) (Greiner Bio-One, Frickenhausen, Germany) and maintained for 24 h at 37 °C. Agonist properties were determined by incubating the test compounds (final range of concentration from 0.1 pM up to 10 μM) in duplicates for 180 min at 37°C. Incubation was stopped by addition of the detection reagents (IP1-d2 conjugate and Anti-IP1cryptate TB conjugate each dissolved in lysis buffer) for further 60 min at room temperature. Time resolved fluorescence resonance energy transfer (HTRF) was measured using the Clariostar plate reader (BMG, Ortenberg, Germany). Data analysis was performed by nonlinear regression using the algorithms for log(agonist) vs. response of PRISM 6.0 (GraphPad, San Diego, CA) and normalization of the raw data to basal (0%) and the maximum effect of dynorphine A (KOR) (100%) (cf. Supporting Information for the corresponding curves).

Recruitment of β-arrestin-2: Measurement of arrestin-2 recruitment was done applying the PathHunter® assay (DiscoverX, Birmingham, U.K.) according to the manufacturer's protocol and as described previously.[90,102] In brief, HEK-293 cells stably expressing the enzyme acceptor (EA) tagged β-arrestin-2 fusion protein were transiently transfected with the ProLink tagged KOR-PK2 construct employing the Mirus TransIT-293 transfection reagent. After 24 h cells were transferred into white clear bottom 384-well plates (5000 cells/well) (Greiner Bio-One) and maintained for further 24 h at 37 °C, 5 % CO_2. To start receptor stimulated arrestin recruitment test compounds were added to the cells to get a final concentration in a range of 1 pM to 10 μM. Incubation was continued for 300 min at 37°C. Stimulation was stopped by addition of the detection mix and further incubation for 60 min at room temperature. Chemiluminescence was

determined using a Clariostar plate reader. Data analysis was done by nonlinear regression using the algorithms for log(agonist) vs. response of PRISM 6.0 (GraphPad, San Diego, CA) and normalization of the raw data to basal (0%) and the maximum effect of dynorphine A (KOR-PK2) (100%) (cf. Supporting Information for the corresponding curves).

Assays on TIRF microscope

  Cell culture: For the binding curves and the single-molecule experiments Chinese Hamster Ovary (CHO) K1 cells (ATCC) were used. Cells were cultured in phenol red-free Dulbecco's modified Eagle's medium (DMEM)/F12 supplemented with 10% (v/v) FBS, 100 U/ml penicillin and 0.1 mg/ml streptomycin at 37°C and 5% CO_2. The cell lines were routinely passaged every two to three days.

  Transfection: CHO-K1 cells were seeded the day before transfection at a density of 1.8 x 10^5 cells per well on clean 25 mm glass coverslips in 6-well culture plates. Transfection was performed with Lipofectamine 2000 according to the manufacturer's protocol. The transfection medium was phenol red-free Dulbecco's modified Eagle's medium (DMEM)/F12 supplemented with 10% (v/v) FBS. For each well 2 µg of human KOR (GenScript) and 6 µL of Lipofectamine 2000 were used.

  Binding curves: The experiments were performed 24 h after transfection. Before imaging each coverslip was incubated for 20 minutes with a specific concentration of fluorescent ligand dissolved in complete medium at 37°C, washed once with 1 mL of imaging buffer (137 mM NaCl, 5.4 mM KCl, 2 mM $CaCl_2$, 1 mM $MgCl_2$, 10 mM HEPES, pH 7.3) and mounted for imaging in a microscopy chamber filled with 300 µL of imaging buffer. Imaging was performed on a custom built TIRF microscope (Cairn Research) based on an Eclipse Ti2 (Nikon, Japan)

equipped with EMCCD cameras (iXon Ultra, Andor), a 561 nm and 637 nm diode lasers, and a 100x oil-immersion objective (NA 1.49, Nikon). Images were acquired using 21 mW laser power (35% of total intensity) of a 637 nm diode laser for the Cy5 compound and 28 mW laser power (35% of total intensity) of a 561 nm diode laser for the Cy3 compound (both lasers from Coherent). TIRF angle was set to 70, exposure time to 47.5 ms. The images were analyzed using ImageJ FIJI. The mean intensity of each cell was averaged over the whole cell and these intensities were then averaged for each ligand concentration. The number of cells for each concentration of ligand was above 30. The intensity of all concentrations was normalized to the intensity of the highest concentration. The averaged fluorescence intensity experimental points were then plotted against ligand concentration and fitted with a nonlinear regression curve fit (log (agonist) vs. response) in PRISM 6.0 (GraphPad, San Diego, CA). Each experiment was replicated three times (cf. Supporting Information for the corresponding curves).

Dissociation kinetics: The experiments were performed 24 h after transfection. Before imaging each coverslip was incubated for 20 minutes at 37°C with 50 nM of fluorescent ligand dissolved in complete medium. After incubation the coverslips were mounted for imaging in a microscopy chamber filled with 300 µL of imaging buffer. The sample was then washed while mounted on the objective by removing the imaging buffer and adding 300 µL of fresh imaging buffer in the microscopic chamber. Imaging was performed on the same customized microscope described previously using 4.8 mW laser power (8% of total intensity), 31.7 ms exposure time and TIRF angle set to 70. Then every minute another picture of the same cell was recorded. As a bleaching control, a movie of 20 frames length was acquired with the same settings as the pictures for the washout in time span of 1 min. The pictures were analyzed using ImageJ FIJI. A region of interest (ROI) was drawn around the cell and from the first image before washing and

then, the same ROI was taken for all following images. The intensity of each cell in each image was measured. Similarly, the movie for the bleaching control was analyzed in each frame. The intensities were then normalized to the initial intensity. Using PRISM 6.0 (GraphPad, San Diego, CA) the intensities were plotted over time and fitted with a one phase exponential decay. Each experiment was replicated three times.

Single Molecule Microscopy

   Methods: CHO-K1 cells (ATCC) were cultured in phenol red-free DMEM/F12, supplemented with 10% FBS at 37 $^{\circ}$C with 5% CO_2. Cells were seeded onto 25 mm clean glass coverslips at a density of 3 x 10^5 per well. On the following day, cells were transfected with the KOR plasmid (cDNA, GenScript), using Lipofectamine 2000, according to the manufacturer's recommendations. Four hours following transfection, KOR transfected cells were labelled with compound **9b** (100 nM) and **9a** (10 nM). After washing the coverslip with 1 mL of imaging buffer (137 mM NaCl, 5.4 mM KCl, 2 mM $CaCl_2$, 1 mM $MgCl_2$, 10 mM HEPES, pH 7.3), the cells were imaged in 300 μL imaging buffer at 20 $^{\circ}$C, using a custom built TIRF microscope (Cairn Research) based on an Eclipse Ti2 (Nikon, Japan) equipped with EMCCD cameras (iXon Ultra, Andor), a 561 nm and 637 nm diode lasers, and a 100x oil-immersion objective (NA 1.49, Nikon). Single-molecule image sequences were acquired with an exposure time of 47.5 ms and using 15 mW laser power (25% of total intensity) of a 637 nm diode laser for the Cy5 compound and 28 mW laser power (35% of total intensity) of a 561 nm diode laser for the Cy3 compound. Control coverslips were co-transfected with KOR and the SNAP-CD86 construct (GenScript). Six hours after transfection they were labelled with 1 μM of SNAP-SiR (New England Biolabs, UK) for 20 mins, followed by 3 x 5 min wash with culture medium. Afterwards, they were

labelled with 100 nM of compound **9b** for 20 mins and then imaged, as previously described, using 24 mW laser power (40% of total intensity) of a 637 nm diode laser for the SiR and 32 mW laser power (40% of total intensity) of a 561 nm diode laser for the Cy3 compound. Image sequences were then analysed with an automated particle detection software (utrack) in the MATLAB environment and further investigated using custom algorithms, as previously described.[91,92]

Analysis: To analyse the motion of receptors, the time-averaged mean squared displacement (TA-MSD)[93] of individual trajectories from TIRF image sequences was computed, as previously described.[92] In order to calculate the diffusion coefficient (D), the TA-MSD data were fitted with the following equation:

$$\text{TA-MSD}(t) = 4Dt^{\alpha} + 4\sigma_{\text{err}}^2$$

where t indicates time, α is the anomalous diffusion exponent and σ_{err} is a constant offset for localization error. Only trajectories lasting at least 100 frames were analysed (10861 trajectories from 24 cells). Trajectories were then categorized according to the diffusion parameters D and α. Particles with $D < 0.01$ $\mu m^2 s^{-\alpha}$ were considered to be immobile. Normal diffusion was assigned to particles that had $D \geq 0.01$ $\mu m^2 s^{-\alpha}$ and $0.75 \leq \alpha \leq 1.25$. Sub- and super-diffusion were assigned to particles with $D \geq 0.01$ $\mu m^2 s^{-\alpha}$ and $\alpha < 0.75$ or $\alpha > 1.25$, respectively.

For the analysis of dimer formation, trajectory segments were first linked to obtain continuous trajectories that are no longer interrupted by merging and splitting events. Then, for each particle in the Cy5 channel at frame f, all particles in Cy3 channel falling within a defined search radius (150 nm) were identified as co-localizing. If a co-localization was also present at frame f+1, the

co-localization was extended. The process was iterated until the last frame of the image sequence. These data were used to build a matrix containing information for each co-localization (involved particles as well as the start and end frames). The observed co-localization time corresponds to the duration of true interactions plus the duration of random co-localizations. Thus, the distribution of the observed co-localization times can be seen as a convolution of the distribution of true interaction times and random co-localization times. The expected distribution for random co-localizations was measured using the KOR (labelled with Cy3 ligand) and a non-interacting protein (CD86). To obtain the true co-localization time, deconvolution with the Lucy-Richardson algorithm was performed.[92]

ASSOCIATED CONTENT

Details about the purification and characterization of the ligands (liquid chromatography elution methods, LCMS reports of target compounds), fluorescence binding curves, intrinsic activity assays. Molecular Formula strings available. This material is available free of charge via the Internet at http://pubs.acs.org

AUTHOR INFORMATION

Corresponding Authors

*michael.decker@uni-wuerzburg.de

*d.calebiro@bham.ac.uk

Author Contributions

All authors have given approval to the final version of the manuscript.

ABBREVIATIONS

Boc, *tert*-butyloxycarbonyl; Cbz, benzyloxycarbonyl; CHO, Chinese hamster ovary; DIPEA, *N,N*-diisopropylethylamine; DMF, dimethylformamide; DOR, delta opioid receptor; EDCI, 1-Ethyl-3-(3-dimethylaminopropyl)carbodiimide; Fmoc, 9-fluorenylmethoxycarbonyl; HEK, human embryonic kidney; HOBt, hydroxybenzotriazole; HPLC, high performance liquid chromatography; KOR, kappa opioid receptor, LCMS, liquid chromatography mass spectrometry; MOR, mu opioid receptor; NOR, nociception receptor; RP, reverse-phased; SAR, structure-activity relationships; TFA, trifluoroacetic acid;

REFERENCES

(1)   Rothstein, M. A. The Opioid Crisis and the Need for Compassion in Pain Management.

Am. J. Public Health **2017**, *107*, 1253–1254.

(2)   Schubert, I.; Ihle, P.; Sabatowski, R. Increase in Opiate Prescription in Germany between 2000 and 2010: A Study Based on Insurance Data. *Dtsch. Arztebl. Int.* **2013**, *110*, 45–51.

(3)   Walwyn, W. M.; Miotto, K. A.; Evans, C. J. Opioid Pharmaceuticals and Addiction: The Issues, and Research Directions Seeking Solutions. *Drug Alcohol Depend.* **2010**, *108*, 156–165.

(4)   Ahlbeck, K. Opioids: A Two-Faced Janus. *Curr. Med. Res. Opin.* **2011**, *27*, 439–448.

(5)   Juurlink, D. N.; Dhalla, I. A. Dependence and Addiction during Chronic Opioid Therapy. *J. Med. Toxicol.* **2012**, *8*, 393–399.

(6)   Trang, T.; Al-Hasani, R.; Salvemini, D.; Salter, M. W.; Gutstein, H.; Cahill, C. M. Pain and Poppies: The Good, the Bad, and the Ugly of Opioid Analgesics. *J. Neurosci.* **2015**, *35*, 13879–13888.

(7)   Dhawan, B. N.; Cesselin, F.; Raghubir, R.; Reisine, T.; Bradley, P. B.; Portoghese, P. S.; Hamon, M. International Union of Pharmacology. XII. Classification of Opioid Receptors. *Pharmacol. Rev.* **1996**, *48*, 567–592.

(8)   Manglik, A.; Kruse, A. C.; Kobilka, T. S.; Thian, F. S.; Mathiesen, J. M.; Sunahara, R. K.; Pardo, L.; Weis, W. I.; Kobilka, B. K.; Granier, S. Crystal Structure of the μ-Opioid Receptor Bound to a Morphinan Antagonist. *Nature* **2012**, *485*, 321–326.

(9)   Granier, S.; Manglik, A.; Kruse, A. C.; Kobilka, T. S.; Thian, F. S.; Weis, W. I.; Kobilka, B. K. Structure of the δ-Opioid Receptor Bound to Naltrindole. *Nature* **2012**, *485*, 400–404.

(10) Wu, H.; Wacker, D.; Mileni, M.; Katritch, V.; Han, G. W.; Vardy, E.; Liu, W.; Thompson, A. A.; Huang, X.-P.; Carroll, F. I.; Mascarella, S. W.; Westkaemper, R. B.; Mosier, P. D.; Roth, B. L.; Cherezov, V.; Stevens, R. C. Structure of the Human κ-Opioid Receptor in Complex with JDTic. *Nature* **2012**, *485*, 327–332.

(11) Thompson, A. A.; Liu, W.; Chun, E.; Katritch, V.; Wu, H.; Vardy, E.; Huang, X.-P.; Trapella, C.; Guerrini, R.; Calo, G.; Roth, B. L.; Cherezov, V.; Stevens, R. C. Structure of the Nociceptin/Orphanin FQ Receptor in Complex with a Peptide Mimetic. *Nature* **2012**, *485*, 395–399.

(12) Cahill, C. M.; Taylor, A. M. W.; Cook, C.; Ong, E.; Moron, J. A.; Evans, C. J. Does the Kappa Opioid Receptor System Contribute to Pain Aversion? *Front. Pharmacol.* **2014**, *5*, 253.

(13) Vanderah, T. W. Delta and Kappa Opioid Receptors as Suitable Drug Targets for Pain. *Clin. J. Pain* **2010**, *26*, S10–S15.

(14) Carroll, F. I.; Carlezon, W. A. Development of κ Opioid Receptor Antagonists. *J. Med. Chem.* **2013**, *56*, 2178–2195.

(15) Kivell, B.; Prisinzano, T. E. Kappa Opioids and the Modulation of Pain. *Psychopharmacology* **2010**, *210*, 109–119.

(16) Eguchi, M. Recent Advances in Selective Opioid Receptor Agonists and Antagonists. *Med. Res. Rev.* **2004**, *24*, 182–212.

(17) Wang, Y.; Sun, J.; Tao, Y.; Chi, Z.; Liu, J. The Role of κ-Opioid Receptor Activation in Mediating Antinociception and Addiction. *Acta Pharmacol. Sin.* **2010**, *31*, 1065–1070.

(18) Butelman, E. R.; Yuferov, V.; Kreek, M. J. κ-Opioid Receptor/Dynorphin System: Genetic and Pharmacotherapeutic Implications for Addiction. *Trends Neurosci.* **2012**, *35*, 587–596.

(19) Metcalf, M. D.; Coop, A. Kappa Opioid Antagonists: Past Successes and Future Prospects. *Am. Assoc. Pharm. Sci. J.* **2008**, *7*, 395–431.

(20) Urbano, M.; Guerrero, M.; Rosen, H.; Roberts, E. Antagonists of the Kappa Opioid Receptor. *Bioorg. Med. Chem. Lett.* **2014**, *24*, 2021–2032.

(21) Lalanne, L.; Ayranci, G.; Kieffer, B. L.; Lutz, P.-E. The Kappa Opioid Receptor: From Addiction to Depression, and Back. *Front. Psychiatry* **2014**, *5*.

(22) Massotte, D. In Vivo Opioid Receptor Heteromerization: Where Do We Stand? *Br. J. Pharmacol.* **2015**, *172*, 420–434.

(23) Fujita, W.; Gomes, I.; Devi, L. A. Revolution in GPCR Signalling: Opioid Receptor Heteromers as Novel Therapeutic Targets: IUPHAR Review 10. *Br. J. Pharmacol.* **2014**, *171*, 4155–4176.

(24) Pin, J.-P.; Neubig, R.; Bouvier, M.; Devi, L.; Filizola, M.; Javitch, J. A.; Lohse, M. J.; Milligan, G.; Palczewski, K.; Parmentier, M.; Spedding, M. International Union of Basic and Clinical Pharmacology. LXVII. Recommendations for the Recognition and Nomenclature of G Protein-Coupled Receptor Heteromultimers. *Pharmacol. Rev.* **2007**, *59*, 5–13.

(25) Che, T.; Majumdar, S.; Zaidi, S. A.; Ondachi, P.; McCorvy, J. D.; Wang, S.; Mosier, P. D.; Uprety, R.; Vardy, E.; Krumm, B. E.; Han, G. W.; Lee, M.-Y.; Pardon, E.; Steyaert, J.;

Huang, X.-P.; Strachan, R. T.; Tribo, A. R.; Pasternak, G. W.; Carroll, F. I.; Stevens, R. C.; Cherezov, V.; Katritch, V.; Wacker, D.; Roth, B. L. Structure of the Nanobody-Stabilized Active State of the Kappa Opioid Receptor. *Cell* **2018**, *172*, 55-67.e15.

(26)   Jordan, B.; Devi, L. G-Protein-Coupled Receptor Heterodimerization Modulates Receptor Function. *Nature* **1999**, *399*, 697–700.

(27)   Chakrabarti, S.; Liu, N.-J.; Gintzler, A. R. Formation of Mu-/Kappa-Opioid Receptor Heterodimer Is Sex-Dependent and Mediates Female-Specific Opioid Analgesia. *Proc. Natl. Acad. Sci. U. S. A.* **2010**, *107*, 20115–20119.

(28)   Liu, N.-J.; Chakrabarti, S.; Schnell, S.; Wessendorf, M.; Gintzler, A. R. Spinal Synthesis of Estrogen and Concomitant Signaling by Membrane Estrogen Receptors Regulate Spinal κ- and μ-Opioid Receptor Heterodimerization and Female-Specific Spinal Morphine Antinociception. *J. Neurosci.* **2011**, *31*, 11836–11845.

(29)   Wang, D.; Sun, X.; Bohn, L.; Sadee, W. Opioid Receptor Homo-and Heterodimerization in Living Cells by Quantitative Bioluminescence Resonance Energy Transfer. *Mol. Pharmacol.* **2005**, *67*, 2173–2184.

(30)   Ramsay, D.; Kellett, E.; McVey, M.; Rees, S.; Milligan, G. Homo- and Hetero-Oligomeric Interactions between G-Protein-Coupled Receptors in Living Cells Monitored by Two Variants of Bioluminescence Resonance Energy Transfer (BRET): Hetero-Oligomers between Receptor Subtypes Form More Efficiently than between Less. *Biochem. J.* **2002**, *365*, 429–440.

(31)   Berg, K. A.; Rowan, M. P.; Gupta, A.; Sanchez, T. A.; Silva, M.; Gomes, I.; McGuire, B.

A.; Portoghese, P. S.; Hargreaves, K. M.; Devi, L. A.; Clarke, W. P. Allosteric Interactions between δ and κ Opioid Receptors in Peripheral Sensory Neurons. *Mol. Pharmacol.* **2012**, *81*, 264–272.

(32)   Evans, R. M.; You, H.; Hameed, S.; Altier, C.; Mezghrani, A.; Bourinet, E.; Zamponi, G. W. Heterodimerization of ORL1 and Opioid Receptors and Its Consequences for N-Type Calcium Channel Regulation. *J. Biol. Chem.* **2010**, *285*, 1032–1040.

(33)   Bhushan, R. G.; Sharma, S. K.; Xie, Z.; Daniels, D. J.; Portoghese, P. S. A Bivalent Ligand (KDN-21) Reveals Spinal Delta and Kappa Opioid Receptors Are Organized as Heterodimers That Give Rise to Delta(1) and Kappa(2) Phenotypes. Selective Targeting of Delta-Kappa Heterodimers. *J. Med. Chem.* **2004**, *47*, 2969–2972.

(34)   Xie, Z.; Bhushan, R. G.; Daniels, D. J.; Portoghese, P. S. Interaction of Bivalent Ligand KDN21 with Heterodimeric δ - κ Opioid Receptors in Human Embryonic Kidney 293 Cells. *Mol. Pharmacol.* **2005**, *68*, 1079–1086.

(35)   Ansonoff, M. A.; Portoghese, P. S.; Pintar, J. E. Consequences of Opioid Receptor Mutation on Actions of Univalent and Bivalent Kappa and Delta Ligands. *Psychopharmacology* **2010**, *210*, 161–168.

(36)   Zhang, S.; Yekkirala, A.; Tang, Y.; Portoghese, P. S. A Bivalent Ligand (KMN-21) Antagonist for μ/κ Heterodimeric Opioid Receptors. *Bioorg. Med. Chem. Lett.* **2009**, *19*, 6978–6980.

(37)   Daniels, D. J.; Kulkarni, A.; Xie, Z.; Bhushan, R. G.; Portoghese, P. S. A Bivalent Ligand (KDAN-18) Containing δ-Antagonist and κ -Agonist Pharmacophores Bridges Δ2 and K1

Opioid Receptor Phenotypes. *J. Med. Chem.* **2005**, *48*, 1713–1716.

(38)   Tang, Y.; Yang, J.; Lunzer, M. M.; Powers, M. D.; Portoghese, P. S. A κ Opioid Pharmacophore Becomes a Spinally Selective κ-δ Agonist When Modified with a Basic Extender Arm. *ACS Med. Chem. Lett.* **2011**, *2*, 7–10.

(39)   Waldhoer, M.; Fong, J.; Jones, R. M.; Lunzer, M. M.; Sharma, S. K.; Kostenis, E.; Portoghese, P. S.; Whistler, J. L. A Heterodimer-Selective Agonist Shows in Vivo Relevance of G Protein-Coupled Receptor Dimers. *Proc. Natl. Acad. Sci. U. S. A.* **2005**, *102*, 9050–9055.

(40)   Yekkirala, A. S.; Lunzer, M. M.; McCurdy, C. R.; Powers, M. D.; Kalyuzhny, A. E.; Roerig, S. C.; Portoghese, P. S. N-Naphthoyl-Beta-Naltrexamine (NNTA), a Highly Selective and Potent Activator of μ/κ-Opioid Heteromers. *Proc. Natl. Acad. Sci. U. S. A.* **2011**, *108*, 5098–5103.

(41)   Calebiro, D.; Sungkaworn, T. Single-Molecule Imaging of GPCR Interactions. *Trends Pharmacol. Sci.* **2018**, *39*, 109–122.

(42)   Calebiro, D.; Jobin, M.-L. Hot Spots for GPCR Signaling: Lessons from Single-Molecule Microscopy. *Curr. Opin. Cell Biol.* **2019**, *57*, 57–63.

(43)   Calebiro, D.; Koszegi, Z. The Subcellular Dynamics of GPCR Signaling. *Mol. Cell. Endocrinol.* **2019**, *483*, 24–30.

(44)   Kusumi, A.; Tsunoyama, T. A.; Hirosawa, K. M.; Kasai, R. S.; Fujiwara, T. K. Tracking Single Molecules at Work in Living Cells. *Nat. Chem. Biol.* **2014**, *10*, 524–532.

(45)   Rahmeh, R.; Damian, M.; Cottet, M.; Orcel, H.; Mendre, C.; Durroux, T.; Sharma, K. S.;

Durand, G.; Pucci, B.; Trinquet, E.; Zwier, J. M.; Deupi, X.; Bron, P.; Baneres, J.-L.; Mouillac, B.; Granier, S. Structural Insights into Biased G Protein-Coupled Receptor Signaling Revealed by Fluorescence Spectroscopy. *Proc. Natl. Acad. Sci.* **2012**, *109*, 6733–6738.

(46) Calebiro, D.; Rieken, F.; Wagner, J.; Sungkaworn, T.; Zabel, U.; Borzi, A.; Cocucci, E.; Zürn, A.; Lohse, M. J. Single-Molecule Analysis of Fluorescently Labeled G-Protein-Coupled Receptors Reveals Complexes with Distinct Dynamics and Organization. *Proc. Natl. Acad. Sci. U. S. A.* **2013**, *110*, 743–748.

(47) Gentzsch, C.; Seier, K.; Drakopoulos, A.; Jobin, M.-L.; Lanoiselée, Y.; Koszegi, Z.; Maurel, D.; Sounier, R.; Hübner, H.; Gmeiner, P.; Granier, S.; Calebiro, D.; Decker, M. Selective and Wash-Resistant Fluorescent Dihydrocodeinone Derivatives Allow Single-Molecule Imaging of μ-Opioid Receptor Dimerization. *Angew. Chemie Int. Ed.* **2020**, DOI: 10.1002/anie.201912683.

(48) Gentzsch, C.; Seier, K.; Drakopoulos, A.; Jobin, M.; Lanoiselée, Y.; Koszegi, Z.; Maurel, D.; Sounier, R.; Hübner, H.; Gmeiner, P.; Granier, S.; Calebiro, D.; Decker, M. Selective and Wash-Resistant Fluorescent Dihydrocodeinone Derivatives Allow Single-Molecule Imaging of M-Opioid Receptor Dimerization. *Angew. Chemie* **2020**, DOI: 10.1002/ange.201912683.

(49) Ma, Z.; Du, L.; Li, M. Toward Fluorescent Probes for G-Protein-Coupled Receptors (GPCRs). *J. Med. Chem.* **2014**, *57*, 8187–8203.

(50) Ciruela, F.; Jacobson, K. A.; Fernández-Dueñas, V. Portraying G Protein-Coupled Receptors with Fluorescent Ligands. *Chem. Biol.* **2014**, *9*, 1918–1928.

(51)   Stoddart, L. A.; Kilpatrick, L. E.; Briddon, S. J.; Hill, S. J. Probing the Pharmacology of G Protein-Coupled Receptors with Fluorescent Ligands. *Neuropharmacology* **2015**, *98*, 48–57.

(52)   Vernall, A. J.; Hill, S. J.; Kellam, B. The Evolving Small-Molecule Fluorescent-Conjugate Toolbox for Class A GPCRs. *Br. J. Pharmacol.* **2014**, *171*, 1073–1084.

(53)   Sridharan, R.; Zuber, J.; Connelly, S. M.; Mathew, E.; Dumont, M. E. Fluorescent Approaches for Understanding Interactions of Ligands with G Protein Coupled Receptors. *Biochim. Biophys. Acta - Biomembr.* **2014**, *1838*, 15–33.

(54)   Iliopoulos-Tsoutsouvas, C.; Kulkarni, R. N.; Makriyannis, A.; Nikas, S. P. Fluorescent Probes for G-Protein-Coupled Receptor Drug Discovery. *Expert Opin. Drug Discov.* **2018**, *13*, 933–947.

(55)   Kolb, V. M.; Koman, A.; Neil, A. Synthesis and Pharmacological Characterization of Fluorescent Opioid Receptor Probes. *Pharm. Res.* **1985**, *02*, 266–271.

(56)   Madsen, B. W.; Beglan, C. L.; Spivak, C. E. Fluorescein-Labeled Naloxone Binding to Mu Opioid Receptors on Live Chinese Hamster Ovary Cells Using Confocal Fluorescent Microscopy. *J. Neurosci. Methods* **2000**, *97*, 123–131.

(57)   Archer, S.; Medzihradsky, F.; Seyed-Mozaffari, A.; Emmerson, P. J. Synthesis and Characterization of 7-Nitrobenzo-2-Oxa-1,3-Diazole (NBD)-Labeled Fluorescent Opioids. *Biochem. Pharmacol.* **1992**, *43*, 301–306.

(58)   Lawrence, D. M. P.; Hutchinson, I.; Seyed-Mozaffari, A.; Archer, S.; Bidlack, J. M. Fluorescent Staining of κ Opioid Receptors Using Naltrexamine Derivatives and

Phycoerythrin. *J. Immunol. Methods* **1997**, *201*, 173–181.

(59) Schembri, L. S.; Stoddart, L. A.; Briddon, S. J.; Kellam, B.; Canals, M.; Graham, B.; Scammells, P. J. Synthesis, Biological Evaluation, and Utility of Fluorescent Ligands Targeting the μ-Opioid Receptor. *J. Med. Chem.* **2015**, *58*, 9754–9767.

(60) Pechulis, A. D.; Archer, S.; Wentland, M. P.; Colasurdo, M.; Bidlack, J. M. Arylacetamide Kappa-Selective Opioid Ligands. *Bioorg. Med. Chem. Lett.* **1997**, *7*, 2271–2276.

(61) Chang, A.-C.; Chao, C.; Takemori, A. E.; Gekker, G.; Hu, S.; Peterson, P. K.; Portoghese, P. S. Arylacetamide-Derived Fluorescent Probes: Synthesis, Biological Evaluation, and Direct Fluorescent Labeling of κ Opioid Receptors in Mouse Microglial Cells. *J. Med. Chem.* **1996**, *39*, 1729–1735.

(62) Lawrence, D. M.; el-Hamouly, W.; Archer, S.; Leary, J. F.; Bidlack, J. M. Identification of Kappa Opioid Receptors in the Immune System by Indirect Immunofluorescence. *Proc. Natl. Acad. Sci. U. S. A.* **1995**, *92*, 1062–1066.

(63) Houghten, R. A.; Dooley, C. T.; Appel, J. R. De Novo Identification of Highly Active Fluorescent Kappa Opioid Ligands from a Rhodamine Labeled Tetrapeptide Positional Scanning Library. *Bioorg. Med. Chem. Lett.* **2004**, *14*, 1947–1951.

(64) Sharma, S. K.; Jones, R. M.; Metzger, T. G.; Ferguson, D. M.; Portoghese, P. S. Transformation of a κ-Opioid Receptor Antagonist to a κ-Agonist by Transfer of a Guanidinium Group from the 5'- to 6'-Position of Naltrindole. *J. Med. Chem.* **2001**, *44*, 2073–2079.

(65) Jones, R. M.; Portoghese, P. S. 5'-Guanidinonaltrindole, a Highly Selective and Potent Kappa-Opioid Receptor Antagonist. *Eur. J. Pharmacol.* **2000**, *396*, 49–52.

(66) Stevens, W. C.; Jones, R. M.; Subramanian, G.; Metzger, T. G.; Ferguson, D. M.; Portoghese, P. S. Potent and Selective Indolomorphinan Antagonists of the Kappa-Opioid Receptor. *J. Med. Chem.* **2000**, *43*, 2759–2769.

(67) Wang, D.; Sun, X.; Sadee, W. Different Effects of Opioid Antagonists on Mu-, Delta-, and Kappa-Opioid Receptors with and without Agonist Pretreatment. *J. Pharmacol. Exp. Ther.* **2007**, *321*, 544–552.

(68) Obara, I.; Mika, J.; Schäfer, M. K.-H.; Przewlocka, B. Antagonists of the κ-Opioid Receptor Enhance Allodynia in Rats and Mice after Sciatic Nerve Ligation. *Br. J. Pharmacol.* **2003**, *140*, 538–546.

(69) Bruchas, M. R.; Yang, T.; Schreiber, S.; Defino, M.; Kwan, S. C.; Li, S.; Chavkin, C. Long-Acting Kappa Opioid Antagonists Disrupt Receptor Signaling and Produce Noncompetitive Effects by Activating c-Jun N-Terminal Kinase. *J. Biol. Chem.* **2007**, *282*, 29803–29811.

(70) Negus, S. S.; Mello, N. K.; Linsenmayer, D. C.; Jones, R.; Portoghese, P. S. Kappa Opioid Antagonist Effects of the Novel Kappa Antagonist 5'-Guanidinonaltrindole (GNTI) in an Assay of Schedule-Controlled Behavior in Rhesus Monkeys. *Psychopharmacology* **2002**, *163*, 412–419.

(71) Casal-Dominguez, J. J.; Clark, M.; Traynor, J. R.; Husbands, S. M.; Bailey, S. J. In Vivo and in Vitro Characterization of Naltrindole-Derived Ligands at the Kappa-Opioid

Receptor. *J. Psychopharmacol.* **2012**, *27*, 192–202.

(72)   Mague, S. D.; Pliakas, A. M.; Todtenkopf, M. S.; Tomasiewicz, H. C.; Zhang, Y.; Stevens, W. C.; Jones, R. M.; Portoghese, P. S.; Carlezon, W. A. Antidepressant-like Effects of Kappa-Opioid Receptor Antagonists in the Forced Swim Test in Rats. *J. Pharmacol. Exp. Ther.* **2003**, *305*, 323–330.

(73)   Munro, T. A.; Berry, L. M.; Van't Veer, A.; Béguin, C.; Carroll, F. I.; Zhao, Z.; Carlezon, W. A.; Cohen, B. M. Long-Acting κ Opioid Antagonists nor-BNI, GNTI and JDTic: Pharmacokinetics in Mice and Lipophilicity. *BMC Pharmacol.* **2012**, *12*, 5.

(74)   Munro, T. A.; Huang, X.-P.; Inglese, C.; Perrone, M. G.; Van't Veer, A.; Carroll, F. I.; Béguin, C.; Carlezon, W. A.; Colabufo, N. A.; Cohen, B. M.; Roth, B. L. Selective κ Opioid Antagonists Nor-BNI, GNTI and JDTic Have Low Affinities for Non-Opioid Receptors and Transporters. *PLoS One* **2013**, *8*, e70701.

(75)   Cheng, J.; Sun, X.; Li, W.; Liu, G.; Tu, Y.; Tang, Y. Molecular Switches of the κ Opioid Receptor Triggered by 6′-GNTI and 5′-GNTI. *Sci. Rep.* **2016**, *6*, 18913.

(76)   Kolinski, M.; Filipek, S. Study of a Structurally Similar Kappa Opioid Receptor Agonist and Antagonist Pair by Molecular Dynamics Simulations. *J. Mol. Model.* **2010**, *16*, 1567–1576.

(77)   Gonçalves, M. S. T. Fluorescent Labeling of Biomolecules with Organic Probes. *Chem. Rev.* **2009**, *109*, 190–212.

(78)   Luo, S.; Zhang, E.; Su, Y.; Cheng, T.; Shi, C. A Review of NIR Dyes in Cancer Targeting and Imaging. *Biomaterials* **2011**, *32*, 7127–7138.

(79)   Ballou, B.; Ernst, L.; Waggoner, A. Fluorescence Imaging of Tumors In Vivo. *Curr. Med. Chem.* **2005**, *12*, 795–805.

(80)   Josan, J. S.; Morse, D. L.; Xu, L.; Trissal, M.; Baggett, B.; Davis, P.; Vagner, J.; Gillies, R. J.; Hruby, V. J. Solid-Phase Synthetic Strategy and Bioevaluation of a Labeled δ-Opioid Receptor Ligand Dmt-Tic-Lys for *In Vivo* Imaging. *Org. Lett.* **2009**, *11*, 2479–2482.

(81)   Huynh, A. S.; Estrella, V.; Stark, V. E.; Cohen, A. S.; Chen, T.; Casagni, T. J.; Josan, J. S.; Lloyd, M. C.; Johnson, J.; Kim, J.; Hruby, V. J.; Vagner, J.; Morse, D. L. Tumor Targeting and Pharmacokinetics of a Near-Infrared Fluorescent-Labeled δ-Opioid Receptor Antagonist Agent, Dmt-Tic-Cy5. *Mol. Pharm.* **2016**, *13*, 534–544.

(82)   Lam, R.; Gondin, A. B.; Canals, M.; Kellam, B.; Briddon, S. J.; Graham, B.; Scammells, P. J. Fluorescently Labeled Morphine Derivatives for Bioimaging Studies. *J. Med. Chem.* **2018**, *61*, 1316–1329.

(83)   Kshirsagar, T.; Nakano, A. H.; Law, P.-Y.; Elde, R.; Portoghese, P. S. NTI4F: A Non-Peptide Fluorescent Probe Selective for Functional Delta Opioid Receptors. *Neurosci. Lett.* **1998**, *249*, 83–86.

(84)   Baker, J. G.; Middleton, R.; Adams, L.; May, L. T.; Briddon, S. J.; Kellam, B.; Hill, S. J. Influence of Fluorophore and Linker Composition on the Pharmacology of Fluorescent Adenosine A1 Receptor Ligands. *Br. J. Pharmacol.* **2010**, *159*, 772–786.

(85)   Vernall, A. J.; Stoddart, L. A.; Briddon, S. J.; Ng, H. W.; Laughton, C. A.; Doughty, S. W.; Hill, S. J.; Kellam, B. Conversion of a Non-Selective Adenosine Receptor Antagonist

into A3-Selective High Affinity Fluorescent Probes Using Peptide-Based Linkers. *Org. Biomol. Chem.* **2013**, *11*, 5673–5682.

(86)   Linton, B. R.; Carr, A. J.; Orner, B. P.; Hamilton, A. D. A Versatile One-Pot Synthesis of 1,3-Substituted Guanidines from Carbamoyl Isothiocyanates. *J. Org. Chem.* **2000**, *65*, 1566–1568.

(87)   Kim, K. S.; Qian, L. Improved Method for the Preparation of Guanidines. *Tetrahedron Lett.* **1993**, *34*, 7677–7680.

(88)   Grodzki, A. C. G.; Poola, B.; Pasupuleti, N.; Nantz, M. H.; Lein, P. J.; Gorin, F. A Novel Carboline Derivative Inhibits Nitric Oxide Formation in Macrophages Independent of Effects on Tumor Necrosis Factor α and Interleukin-1β Expression. *J. Pharmacol. Exp. Ther.* **2015**, *352*, 438–447.

(89)   Broach, J. R.; Thorner, J. High-Throughput Screening for Drug Discovery. *Nature* **1996**, *384*, 14–16.

(90)   Liu, H.; Hofmann, J.; Fish, I.; Schaake, B.; Eitel, K.; Bartuschat, A.; Kaindl, J.; Rampp, H.; Banerjee, A.; Hübner, H.; Clark, M. J.; Vincent, S. G.; Fisher, J. T.; Heinrich, M. R.; Hirata, K.; Liu, X.; Sunahara, R. K.; Shoichet, B. K.; Kobilka, B. K.; Gmeiner, P. Structure-Guided Development of Selective M3 Muscarinic Acetylcholine Receptor Antagonists. *Proc. Natl. Acad. Sci. U. S. A.* **2018**, *115*, 12046–12050.

(91)   Jaqaman, K.; Loerke, D.; Mettlen, M.; Kuwata, H.; Grinstein, S.; Schmid, S. L.; Danuser, G. Robust Single-Particle Tracking in Live-Cell Time-Lapse Sequences. *Nat. Methods* **2008**, *5*, 695–702.

(92) Sungkaworn, T.; Jobin, M.-L.; Burnecki, K.; Weron, A.; Lohse, M. J.; Calebiro, D. Single-Molecule Imaging Reveals Receptor–G Protein Interactions at Cell Surface Hot Spots. *Nature* **2017**, *550*, 543–547.

(93) Lanoiselée, Y.; Sikora, G.; Grzesiek, A.; Grebenkov, D. S.; Wyłomańska, A. Optimal Parameters for Anomalous-Diffusion-Exponent Estimation from Noisy Data. *Phys. Rev. E* **2018**, *98*, 062139.

(94) Jiang, Y.; Yuan, Y.; Zhang, X.; Liang, T.; Guo, Y.; Li, M.; Pu, X. Use of Network Model to Explore Dynamic and Allosteric Properties of Three GPCR Homodimers. *RSC Adv.* **2016**, *6*, 106327–106339.

(95) Kaczor, A. A.; Guixà-González, R.; Carrió, P.; Poso, A.; Dove, S.; Pastor, M.; Selent, J. Multi-Component Protein - Protein Docking Based Protocol with External Scoring for Modeling Dimers of G Protein-Coupled Receptors. *Mol. Inform.* **2015**, *34*, 246–255.

(96) Filizola, M.; Weinstein, H. Structural Models for Dimerization of G-Protein Coupled Receptors: The Opioid Receptor Homodimers. *Biopolymers* **2002**, *66*, 317–325.

(97) Provasi, D.; Boz, M. B.; Johnston, J. M.; Filizola, M. Preferred Supramolecular Organization and Dimer Interfaces of Opioid Receptors from Simulated Self-Association. *PLOS Comput. Biol.* **2015**, *11*, e1004148.

(98) Hübner, H.; Haubmann, C.; Utz, W.; Gmeiner, P. Conjugated Enynes as Nonaromatic Catechol Bioisosteres: Synthesis, Binding Experiments, and Computational Studies of Novel Dopamine Receptor Agonists Recognizing Preferentially the D3 Subtype. *J. Med. Chem.* **2000**, *43*, 756–762.

(99)   Fish, I.; Stößel, A.; Eitel, K.; Valant, C.; Albold, S.; Huebner, H.; Möller, D.; Clark, M. J.; Sunahara, R. K.; Christopoulos, A.; Shoichet, B. K.; Gmeiner, P. Structure-Based Design and Discovery of New M2 Receptor Agonists. *J. Med. Chem.* **2017**, *60*, 9239–9250.

(100) Lowry, O. H.; Rosebrough, N. J.; Farr, A. L.; Randall, R. J. Protein Measurement with the Folin Phenol Reagent. *J. Biol. Chem.* **1951**, *193*, 265–275.

(101) Cheng, Y.; Prusoff, W. H. Relationship between the Inhibition Constant (K1) and the Concentration of Inhibitor Which Causes 50 per Cent Inhibition (I50) of an Enzymatic Reaction. *Biochem. Pharmacol.* **1973**, *22*, 3099–3108.

(102) Hübner, H.; Schellhorn, T.; Gienger, M.; Schaab, C.; Kaindl, J.; Leeb, L.; Clark, T.; Möller, D.; Gmeiner, P. Structure-Guided Development of Heterodimer-Selective GPCR Ligands. *Nat. Commun.* **2016**, *7*, 12298.

TOC
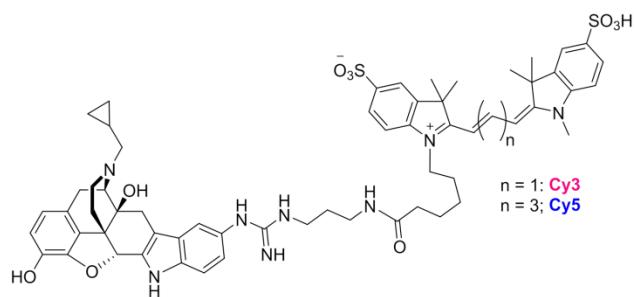
Single Molecule Microscopy
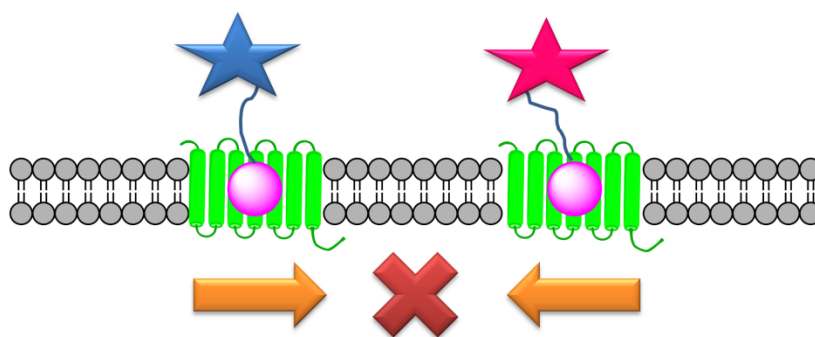
No κOR homodimer formation detected with TIRF microscopy